materials

MDPI

Article

Critical Insight into Pretransitional Behavior and Dielectric Tunability of Relaxor Ceramics

Sylwester J. Rzoska [1], Aleksandra Drozd-Rzoska [1,*], Weronika Bulejak [2,*], Joanna Łoś [1], Szymon Starzonek [3], Mikołaj Szafran [2] and Feng Gao [4]

[1] Institute of High-Pressure Physics Polish Academy of Sciences, ul. Sokołowska 29/37, 01-142 Warsaw, Poland; sylwester.rzoska@unipress.waw.pl (S.J.R.); joalos@unipress.waw.pl (J.Ł.)
[2] Faculty of Chemistry, Warsaw University of Technology, Noakowskiego 3, 00-664 Warsaw, Poland; mikolaj.szafran@pw.edu.pl
[3] Laboratory of Physics, Faculty of Electrical Engineering, University of Ljubljana, Tržaška 25, 1000 Ljubljana, Slovenia; szymon.starzonek@fe.uni-lj.si
[4] State Key Laboratory of Solidification Processing, MIIT Key Laboratory of Radiation Detection Materials and Devices, NPU-QMUL Joint Research Institute of Advanced Materials and Structures (JRI-AMAS), School of Materials Science and Engineering, Northwestern Polytechnical University, Xi'an 710072, China; gaofeng@nwpu.edu.cn
* Correspondence: arzoska@unipress.waw.pl (A.D.-R.); weronika.bulejak.dokt@pw.edu.pl (W.B.)

Abstract: This model discussion focuses on links between the unique properties of relaxor ceramics and the basics of Critical Phenomena Physics and Glass Transition Physics. It indicates the significance of uniaxiality for the appearance of mean-field type features near the paraelectric-to-ferroelectric phase transition. Pretransitional fluctuations, that are increasing up to the size of a grain and leading to inter-grain, random, local electric fields are responsible for relaxor ceramics characteristics. Their impact yields the pseudospinodal behavior associated with "weakly discontinuous" local phase transitions. The emerging model redefines the meaning of the Burns temperature and polar nanoregions (PNRs). It offers a coherent explanation of "dielectric constant" changes with the "diffused maximum" near the paraelectric-to-ferroelectric transition, the sensitivity to moderate electric fields (tunability), and the "glassy" dynamics. These considerations are challenged by the experimental results of complex dielectric permittivity studies in a $Ba_{0.65}Sr0._{35}TiO_3$ relaxor ceramic, covering ca. 250 K, from the paraelectric to the "deep" ferroelectric phase. The distortion-sensitive and derivative-based analysis in the paraelectric phase and the surrounding paraelectric-to-ferroelectric transition reveal a preference for the exponential scaling pattern for $\varepsilon(T)$ changes. This may suggest that Griffith-phase behavior is associated with mean-field criticality disturbed by random local impacts. The preference for the universalistic "critical & activated" evolution of the primary relaxation time is shown for dynamics. The discussion is supplemented by a coupled energy loss analysis. The electric field-related tunability studies lead to scaling relationships describing their temperature changes.

Keywords: relaxor ceramics; dielectric properties; critical phenomena; glassy dynamics; modeling

check for updates

Citation: Rzoska, S.J.; Drozd-Rzoska, A.; Bulejak, W.; Łoś, J.; Starzonek, S.; Szafran, M.; Gao, F. Critical Insight into Pretransitional Behavior and Dielectric Tunability of Relaxor Ceramics. *Materials* **2023**, *16*, 7634. https://doi.org/10.3390/ma16247634

Academic Editors: Francesco Baino and Maziar Montazerian

Received: 18 October 2023
Revised: 22 November 2023
Accepted: 27 November 2023
Published: 13 December 2023

Copyright: © 2023 by the authors. Licensee MDPI, Basel, Switzerland. This article is an open access article distributed under the terms and conditions of the Creative Commons Attribution (CC BY) license (https://creativecommons.org/licenses/by/4.0/).

1. Introduction

Relaxor ceramics remain a cognitive challenge despite seven decades of research [1–54]. The significance of innovative applications extends from varactors, signal tunable filters, phase shifters, and frequency-selective surfaces for conformal antennas to possible electrocaloric effect applications [12,14,16,21,27,28,34,35,41,45–51]. Their unique dielectric properties, sensitivity to the external electric field, and tunability are essential. The increase in research reports since 2020 (24% rise in 2022 and 70% increase, up to approximately 3600 papers in 2023 [52]) shows the significance of relaxor ceramics. Regarding relaxor ceramics applications, the global market is expected to quadruple between 2022 and 2029 to approximately USD 16 billion [52,53].

The unique properties of relaxor ceramics are mainly related to their 'dielectric constant' changes near the paraelectric-to-ferroelectric transition. The "homogeneous," canonic ferroelectric material is crucial as a reference case. In such a system, the temperature dependence of the dielectric constant $\varepsilon(T)$ is represented by the Curie–Weiss (CW) equation [2–5,7,9–12,14,16,19,21,24,25,28,33–35,38,41,43]:

$$\varepsilon(T) = \frac{A_{CW}}{T - T_C}, \tag{1a}$$

$$\Rightarrow \frac{1}{\varepsilon(T)} = A_{CW}^{-1} T - A_{CW}^{-1} T_C, \tag{1b}$$

where $A_{CW} = const$ and T_C is the Curie–Weiss critical temperature.

For inherently "heterogeneous" relaxor ceramics, instead of the "infinite" singularity $\varepsilon(T \to T_C) \to \infty$ (Equation (1a,b)), a "diffused" temperature maximum of $\varepsilon(T)$ appears [1–54]. The next unique feature is related to strong changes in the dielectric constant when even a moderate external electric field is applied. This is described by the so-called tunability (T%) [9,12,14–16,24,25,27,28,34–36,41,43]:

$$T(\%) = \frac{\varepsilon(E \to 0) - \varepsilon(E)}{\varepsilon(E \to 0)} \times 100\%. \tag{2}$$

The dynamics of relaxor ceramics exhibit scaling patterns characteristic of glass-forming systems in the previtreous domain. The hallmark of "glassy" dynamics is the super-Arrhenius (SA) temperature evolution of the primary relaxation time, for which the Vogel–Fulcher–Tammann (VFT) dependence is used as the main replacement equation [1–52]:

$$\tau(T) = \tau_\infty exp \frac{E_a(T)}{RT}, \tag{3a}$$

$$\Rightarrow \tau(T) = \tau_\infty exp \frac{D}{T - T_0} = \tau_\infty exp \frac{D_T T_0}{T - T_0}. \tag{3b}$$

Equation (3a) is the canonic SA relation, with the apparent (temperature-dependent) activation energy $E_a(T)$. Equation (3a) simplifies to the basic Arrhenius equation for $E_a(T) = E_a = const$, in the given temperature domain. R denotes the gas constant.

For the VFT model equation: $E_a(T) = Dt = (RD_T T_0)t^{-1}$, and $t = (T - T_0)/T$ represents the relative distance from the extrapolated singular VFT temperature T_0. In glass-forming systems, T_0 is located below the glass temperature T_g, which by "convention" is linked to $\tau(T_g) = 100s$. The amplitude $D = const$ and D_T is called the fragility strength [54–56].

Broadband dielectric spectroscopy (BDS) is essential for determining the mentioned properties [55]. BDS output results can be represented as the complex dielectric permittivity: $\varepsilon^*(f,T) = \varepsilon'(f,T) - i\varepsilon''(f,T)$. The real part, $\varepsilon'(f,T)$, enables the determination of the canonic dielectric constant. It is associated with the so-called static domain of $\varepsilon'(f, T = const)$ spectrum, where a frequency shift does not significantly change the dielectric permittivity value. For dipolar dielectrics, it occurs within the 1 kHz $< f <$ 10 MHz domain. For lower frequencies (LF), below the static domain, a strong increase in $\varepsilon'(f)$ and $\varepsilon''(f)$ occurs, which is commonly linked to the impact of ionic contamination [55]. The response related to relaxation processes appears in higher frequencies, above the static domain [55].

In relaxor systems, for temperature changes in the dielectric constant, $\varepsilon'(T, f = const)$, the diffused maximum near the paraelectric-to-ferroelectric transition is the characteristic feature. Its "branches" are described by the CW relation (Equation (1)) for a set of scanned frequencies. Parameters describing the maximum, $(\varepsilon'_{max}, \varepsilon_m)$ and (T_{max}, T_m), are frequency-dependent [1–52]. This indicates that for relaxors, one should consider the real part of the dielectric permittivity rather than the canonic dielectric constant.

Regarding dynamics, the primary loss curve $\varepsilon''(f, T = const)$ characterizing the relaxation process associated with permanent dipole moments is significant. Its time scale esti-

mates the peak frequency, namely the primary relaxation time: $\tau = 1/\omega_{peak} = 1/2\pi f_{peak}$ [56]. For ferroelectric systems, including relaxors, temperature scans for subsequent frequencies lead to the manifestation of primary loss curves in $\varepsilon''(f = const, T)$ plane. In this case, experimental data are portrayed via the following relation [1–3,7–10,12–14,21,24,32,35,47]:

$$f(T) = f(T_m) = f_\infty exp\frac{E_a'(T)}{T} = f_\infty exp\frac{D'}{T_m - T_0}, \quad (4)$$

where T_m is the temperature for the maximum of $\varepsilon''(f = const, T)$ detected in temperature scans for subsequent frequencies f; $T_m = T_{max}$ is the temperature describing the loss curve maximum for such scans.

Equation (3a,b) convert into Equation (4) for $\tau(T) \to 1/f(T)$ and $T \to T_m$.

The "glassy", "previtreous"-type dynamics is also associated with the non-Debye, multi-time distribution of relaxation times. It is manifested by the "broadening" of the primary loss curves above the single-relaxation-time Debye pattern. Most commonly, it is represented via the Havriliak–Negami (HN) relation [3,4,9,12–14,16–19,21,24,29–33,47,54–56]:

$$\varepsilon^*(f) = \varepsilon_\infty + \frac{\Delta\varepsilon}{\left(1 + (i\omega\tau)^a\right)^b} \quad (5)$$

where power exponent $0 < a, b < 1$.

When $a, b = 1$, Equation (5) is simplified to the basic Debye equation associated with a single relaxation time. In Equation (5), $\Delta\varepsilon = \varepsilon - \varepsilon_\infty$ is called the dielectric strength and describes the dipolar contribution to the "total" value of the dielectric constant; ε_∞ is the non-dipolar permittivity related to electronic and atomic contributions.

Studies in supercooled glass-forming liquids have shown that the power exponents in Equation (5) can be used as metrics for the distribution of primary relaxation times. It is well illustrated by the Jonsher scaling [57] of primary loss curves $\varepsilon''(f,\ T = const)$ [56,58]:

$$\frac{\varepsilon''(f < f_{max})}{\varepsilon''_{max}} = a\prime f^m \ \Rightarrow\ log_{10}\left(\varepsilon''(f)/\varepsilon''_{max}\right) = log_{10}a\prime + mlog_{10}f, \quad (6a)$$

$$\frac{\varepsilon''(f > f_{max})}{\varepsilon''_{max}} = b\prime f^{-n} \ \Rightarrow\ log_{10}\left(\varepsilon''(f)/\varepsilon''_{max}\right) = log_{10}b\prime - nlog_{10}f, \quad (6b)$$

where $T = const$, $a\prime, b\prime = const$, and $m,\ n$ are parameters describing the distribution.

The following link between the distribution metric for HN Equation (5) and Jonsher Equation (6) takes place: $m = a$ and $n = ab$. The reference Debye relaxation is related to $m = n = 1$.

The analysis based on Equation (6a,b) enables the reliable determining of the relaxation time, using the condition: $dlog_{10}(\varepsilon''(f))/dlog_{10}f = 0$, for $f = f_{peak}$ and $\tau = 1/2\pi f_{peak}$. Alternatively, the relaxation time can be determined using the HN Equation (5), but it is associated with the five-parameter nonlinear fitting.

For glass-forming systems, the SA (Equation (3a,b)) and the non-Debye (Equation (5)) behavior take place on cooling from the ultraviscous/ultraslowed domain to the amorphous solid glass. It is associated with the time-scale $\tau(T_g) \sim 100s$ [58]. For relaxor systems, the transition is associated with the "diffused" paraelectric–ferroelectric transition, and the mentioned "glassy" time scale is not reached [1–52].

It should be stressed that such features of the complex dynamics are absent for basic "homogeneous" ferroelectric systems.

In relaxor ceramics, the temperature at which the distortion from the CW behavior (Equation (1a,b)) occurs on cooling towards the transition is called the Burns temperature (T_B) [3,4]. It is linked to the onset of polar nanoregions (PNRs), a key concept to explain unique relaxors' features [3–54]. It is noted that [37] *"(. . .) the emergence of PNRs begins to form rapidly through the interaction among adjacent dipoles and orients between the states with the same energy and contributes less to the dielectric permittivity because of violent thermal fluctuation"*. It is suggested that the enhanced interactions between the dipole clusters increase the

correlation length, supporting the PNR-associated local field properties. The electric field can reorient the PNRs, which can significantly change the dielectric permittivity behavior, characterized by the aforementioned deviation from the Curie–Weiss law. Following this picture, the "microscopic fluctuations", in which local fluctuations, associated with the PNRs, cause local changes in the Curie temperature T_C, often heuristically commented as the consequence of local concentration changes, have been introduced [2,4–14,16,18,20,21,24–26,31–39,47]. Assuming a Gaussian-type distribution of T_C, Uchino and Nomura proposed the following relation to describe the dielectric constant changes in relaxor ceramics [2,24]:

$$\frac{1}{\varepsilon(T)} = \frac{1}{\varepsilon_m} exp\left(-\frac{(T-T_A)^2}{2\sigma^2}\right) \approx \frac{1}{\varepsilon_m}\left[1 + \frac{(T-T_A)^2}{2\sigma^2} + \ldots\right], \quad (7)$$

for $T > T_m$, $\varepsilon_m = \varepsilon_{max}$. Uchino and Nomura proposed the assumption of $T_A = T_m$ and generalize the above relation to arbitrary power exponent $1 \leq \gamma \leq 2$, which led to the commonly used semi-empirical relation [24]:

$$\frac{1}{\varepsilon(T)} - \frac{1}{\varepsilon_m} = C'^{-1}(T - T_m)^{\gamma\prime}. \quad (8)$$

The above relation can be used to represent experimental data in the paraelectric phase, even for $T - T_m > 1 \div 3K$ [2,4–14,16,18,20,21,24–26,31–39,42–44]. It should be emphasized that Equation (8) "reduces" to CW Equation (1) for $\gamma = 1$. It leads to the conclusion that in such a case $\gamma' \to 1$ and $T_m \to T_C$, $\varepsilon_m \to \infty$. However, in the opinion of the authors, the link between the exponent γ' in Equation (8) and well-defined critical exponents [59–64] is not clear.

In ref. [7], a different pattern of dielectric constant changes was proposed. The model considered the impact of relaxation polarization processes associated with PNRs by introducing two contributions. The first is due to the thermally activated flips of the polar regions, and the second represents the "other" polarization process. The following relation was obtained for $T > T_m$ [7]:

$$\varepsilon(T) = \varepsilon_\infty + \varepsilon_{ref.} exp(a - bT), \quad (9)$$

where in the given case parameters $a, b = const$, and the coefficient b is related to the rate of PNRs in the material.

The behavior in the ferroelectric state, for $T < T_m$, was also derived [7]:

$$\varepsilon(T) = \varepsilon_\infty + A(T)(ln\omega_0 - ln\omega), \quad (10)$$

where ω_0 is the average relaxation frequency of a polar unit cell that is independent of the temperature, i.e., $ln\omega_0 = const$, $A(T)$ is an intrinsic parameter of the relaxor material.

Notwithstanding, experimental results for relaxor systems are commonly scaled via Equations (7) or (8) or their parallels.

The reorientation of the PNRs, characterized by the relaxation time (τ), is also the reference for models focused on the non-Arrhenius behavior of the primary relaxation time, for which the VFT relation is used as the scaling reference. For the authors, a problem arises when taking into account that the PNRs concept is coupled to the Burns temperature, i.e., the onset of the distortion from the CW behavior on cooling towards the paraelectric–ferroelectric transition, whereas the glassy dynamics, represented by Equation (3), are observed on both sides of T_B [1–52].

Despite decades of studies, a commonly accepted model to explain the aforementioned characteristics of relaxor ceramics is still lacking [1–52]. The combination of "glassy" dynamics and the "distorted critical-like" behavior (Equations (1) and (7)) remains a challenge. Even the coherent addressing of the canonical experimental features mentioned above, which are checkpoints for theoretical models, remains a problem. Simple and

fundamentally justified scaling dependencies support relaxor ceramics' modeling, and they can be crucial for the expected boost in innovative relaxor-based devices [52,53].

In this report, we propose looking at the discussed properties of relaxor materials from a slightly different perspective, namely with an explicit reference to the basics of *Critical* Phenomena and Phase Transitions Physics [59–62] and Glass Transition Physics [54–56] and then confront the emerging conclusions with existing and new experimental results, also based on research carried out specifically for this work.

2. Materials and Methods

The BST sample was prepared using $BaCO_3$ (>98%, Chempur, Piekary Śląskie, Poland), $SrCO_3$ (>98%, Chempur, Piekary Śląskie, Poland), and TiO_2 rutile (>99.9%, Sigma-Aldrich, St. Louis, MO, USA). The materials in stoichiometric proportions ($Ba_{0.65}Sr_{0.35}TiO_3$) were ball-milled for 7 h in water and ethanol, subsequently dried and calcined at 1050 °C for 2 h, and finally, barium strontium titanate was synthesized in a high-temperature solid-state reaction carried out at 1340 °C for 2 h. The sintered material was ground with water and zirconia grinding media on a Witeg BML-6 ball mill at a speed of 300 rpm for 7 h. After drying, the samples of diameter d = 20 mm and height h = 5 mm were obtained via pressing and sintering at 1300 °C for 1 h.

The densities of the samples were measured using a helium pycnometer AccuPyc II 1340 (Micromeritics, Norcross, GA, USA). The density of the synthesized powder was 5.629 ± 0.004 g/cm^3, while the density of the sintered sample was 5.612 ± 0.005 g/cm^3.

The average particle size measurements were performed using a Laser Scattering Particle Size Distribution Analyzer LA-950 (HORIBA, Kyoto, Japan). Figure 1 shows the particle size distribution of synthesized barium strontium titanate powder. The average particle size was 1.88 μm.

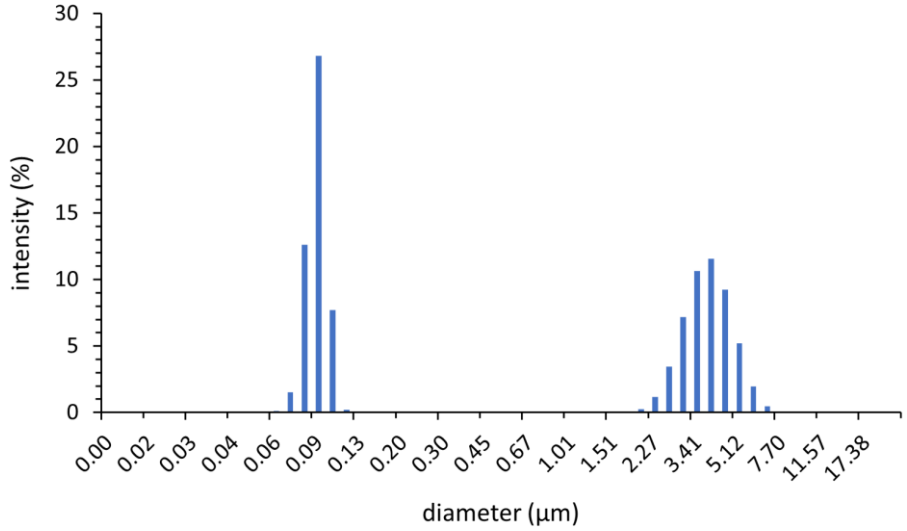

Figure 1. Results of particle size distribution analysis.

The powder consists of two fractions: small particles (0.06–0.13 μm) and larger agglomerates (2–7 μm), which were probably formed by the re-aggregation of small particles during the milling process. The powder X-ray diffraction patterns were recorded at room temperature on an X'PERT PRO MPD X-ray diffractometer (Panalytical, Almelo, The Netherlands) with a Cu anode. An X-ray diffractogram was made in the angular 2θ range from 5 to 81° for the powder sample and used to identify the phase composition. It was quantitatively analyzed using the Rietveld method, which was also employed to calculate the size of the crystallites.

A sample holder with a spinner was used in this study. The size of the crystallites and lattice distortions were determined directly from the Sherrer equation for 110 BST reflex. The coarse-crystalline calcite of natural origin and its reflex 104 were used as a half-width standard for the measuring system. The unit cell parameters were refined

using the Rietveld method in quantitative analysis. The results of XRD qualitative and quantitative analysis are shown in Table 1. The synthesized BST consisted of 99.3% BST in the assumed stoichiometry ($Ba_{0.65}Sr_{0.35}TiO_3$), including cubic (77.1%) and tetragonal (22.9%) phases, and a small (below 1%) addition of cubic $BaTiO_3$.

Table 1. The composition, structure, and size of the tested relaxor ceramic crystallites.

Composition	Share (%)	Crystalline Structure Type	The Share of the Given CS Type %
$Ba_{0.65}Sr_{0.35}TiO_3$	99.3	Cubic	77.1
		Tetragonal	22.9
$BaTiO_3$	0.7	Cubic	100

Based on the microstructural observations of the sintered sample (Figure 2) performed with a scanning electron microscope Prisma E (Thermo Scientific, Waltham, MA, USA), the grains grew approximately five times larger. During the sintering process of the agglomerates, pores and grain boundaries disappear so that we can observe sintered agglomerates with a size in the range of 2–10 µm in the sample structure. The visible defects in the sample were probably caused by the grains being torn out when breaking the sample for observations.

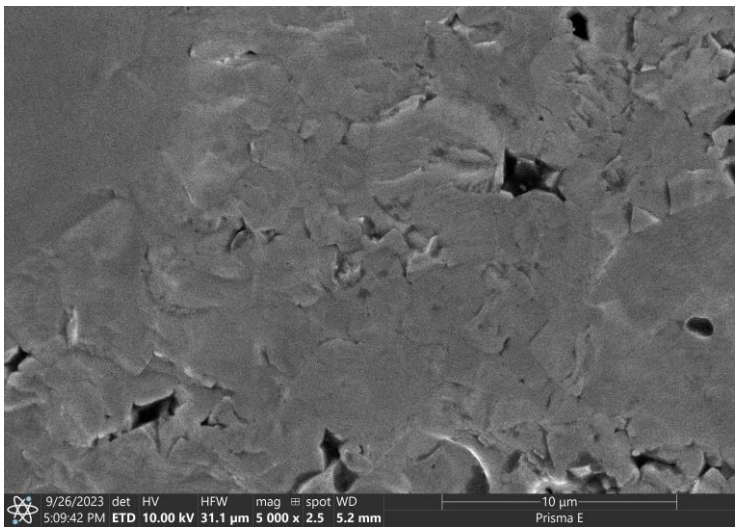

Figure 2. Scanning electron microscope picture of the sintered tested ceramic sample.

The ceramic samples were then sliced into discs of height h = 1 mm for broadband dielectric spectroscopy (BDS) studies [55]. These were carried out using a Novocontrol Alpha-A spectrometer (NOVOCONTROL Technologies GmbH & Co. KG, Montabaur, Germany), which allows for high-resolution studies up to 5–6 of digits permanent resolution over a broad frequency and temperature ranges. The latter was controlled using a Novocontrol Quattro system. The adjustment of the system elements made by the manufacturer allows for the removal of all parasitic capacitances and the direct registration in the representation of the dielectric permittivity: $\varepsilon^*(f,T) = \varepsilon' - i\varepsilon''$. The results were recorded isothermally for about 63 different frequencies for 250 temperatures tested successively. It made it possible to analyze the data in the representation $\varepsilon^*(f, T = const)$ as shown in Figure 3, commonly used in Critical Phenomena Physics [59–62] and Glass Transition Physics [54–58] and in the equivalent representation $\varepsilon^*(f = cont, T)$ (Figure 4) often used in the physics of ferroelectrics [63–68] and relaxors [1–52].

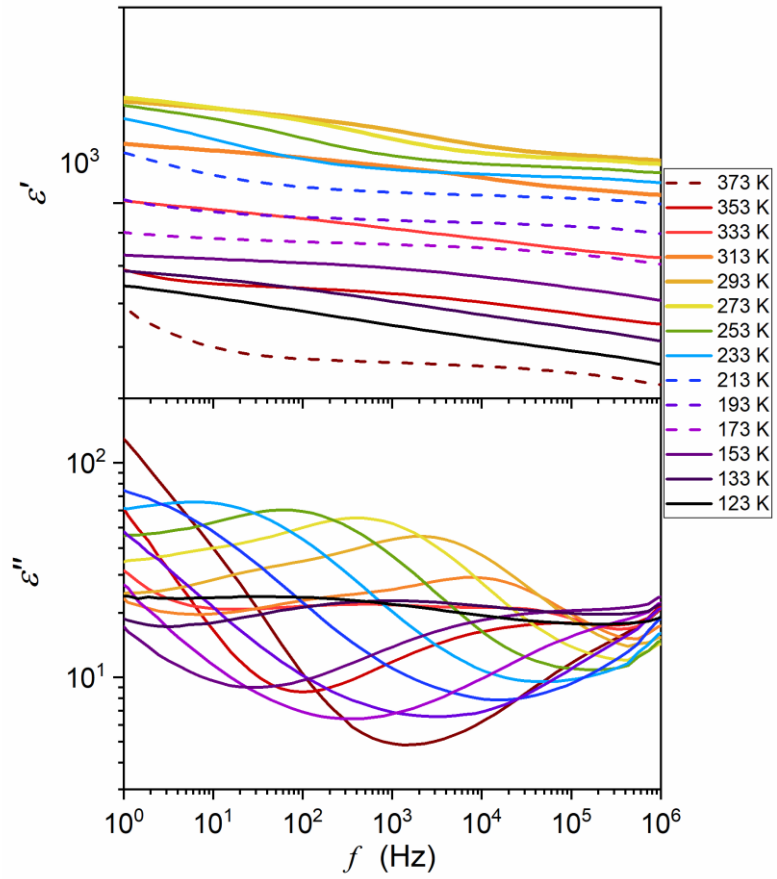

Figure 3. BDS-related spectra showing frequency evolution for the real and imaginary part of the dielectric permittivity (log-log scale), for selected temperatures in the tested ceramic specified in Table 1. The complete data set comprises 250 tested temperatures (see Appendix A).

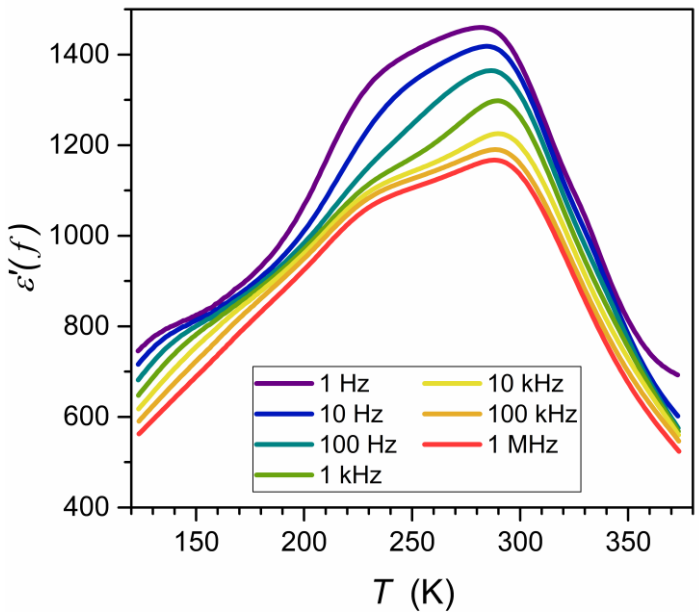

Figure 4. Temperature evolutions of the real part of dielectric permittivity for selected frequencies in the tested relaxor ceramic, specified in Table 1. See also Appendix A.

3. Results

3.1. Model Discussion

3.1.1. "Critical" View on Dielectric-Constant-Related Behavior in Relaxor Systems

The Curie–Weiss (CW) type scaling of dielectric constant temperature evolution is the essential experimental reference for basic "homogeneous" ferroelectrics and related "complex & heterogeneous" ferroelectric relaxor systems [1–52]. To interpret the CW-type behavior [69–71], Devonshire [72,73] directly used the Landau model [74], which considers the free energy power series expansion of the order parameter as the metric of the appearing/disappearing symmetry elements near the continuous phase transitions. Taking the electric polarization P as the order parameter, one obtains [72,73]:

$$F = F_0 + \frac{a}{2}P^2 + \frac{b}{4}P^4 + \frac{c}{6}P^6 - EP, \tag{11}$$

where coefficient $a = A(T - T_C)$; parameters b and c are considered approximately constant. The last term reflects the interaction with the electric field.

The above relation includes the $\frac{c}{6}P^6$ term, characteristic for the tricritical point (TCP) case, the simplest multicritical point associated with meeting three critical points curves [60,61]. The so-called symmetric TCP manifests via the smooth crossover from discontinuous to continuous phase transitions [61]. This term is absent for the basic mean-field (MF) case [60,61]. Equation (11) gives the following pattern for pretransitional changes in the order parameter [59–62,74–76]:

$$P(T) \propto (T_C - T)^{\beta}. \tag{12}$$

The exponent $\beta = 1/2$ for MF and $\beta = 1/4$ for TCP [60]. For the susceptibility, i.e., the order parameter changes via the coupled external field, $\chi = dP/dE$:

$$\chi(T) = \frac{a^{-1}}{(T - T_C)^{\gamma}}, \text{ for } T > T_C, \tag{13a}$$

$$\chi(T) = \frac{(2a)^{-1}}{(T_C - T)^{\gamma}}, \text{ for } T < T_C. \tag{13b}$$

The susceptibility-related exponent $\gamma = 1$, both for MF and TCP cases.

Equation (11) leads to the prediction of linear heat capacity changes on both sides of T_C, i.e., no pretransitional anomaly associated with (critical) exponents but instead only the "jump": $\Delta C_v = T_C a^2/2b$ [61,74]. This behavior does not correlate with experimental results, for which heat capacity pretransitional anomalies have been evidenced [12,14,19]. The basic Landau–Devonshire model dependence (Equation (11)) [72,73], or generally the basic Landau model [74], which originally was exemplified for magnetization and paramagnetic-ferromagnetic transition, is related to the "classical" behavior within the basic MF or TCP approximations, with a hypothetical negligible impact of pretransitional/precritical fluctuations. Nevertheless, such an impact exists. To show it explicitly, Ginzburg supplemented the Landau equation with the gradient term [77,78], which directly recalls fluctuations. Implementing this concept to Equation (11), one obtains:

$$F = F_0 + \frac{a}{2}P^2 + \frac{b}{4}P^4 + \frac{c}{6}P^6 + \kappa(\nabla P)^2 - EP, \tag{14}$$

where κ is the stiffness coefficient and the term $(\nabla P)^2 \propto \langle \delta P^2 \rangle$ is related to fluctuations of the order parameter around some "equilibrium" value.

Equation (14) or its parallels for isomorphic critical systems yield temperature characterizations of the correlation length (size) ξ and the lifetime $\tau_{fl.}$ of pretransitional/precritical fluctuations [61]:

$$\xi(T) = \xi_0 |T - T_C|^{-\nu}, \tag{15a}$$

$$\tau_{fl.}(T) = \tau_0 |T - T_C|^{-\varphi} \propto [\xi(T)]^z, \tag{15b}$$

where ν is the correlation length critical exponent, $\phi = z\nu$; z is the so-called dynamic exponent: $z = 2$ for the conserved order parameter and $z = 3$ for the non-conserved order parameter. For the classic behavior (MF, TCP), $\nu = 1/2$ and $\phi = 1$.

Equation (14) leads to the following pretransitional behavior of the heat capacity [61]:

$$C_v(T \to T_C) \propto |T - T_C|^{-\alpha}, \tag{16}$$

with exponents $\alpha = 1/2$ ($T < T_C$) and $\alpha = 0$ ($T > T_C$) for MF; for TCP, $\alpha = 1/2$ both for $T < T_C$ and $T > T_C$.

Critical exponents are basic parameters characterizing pretransitional behavior. The grand success of Critical Phenomena Physics [59–62] was related to showing that the values of critical exponents depend only on the space (d) and the order parameter (n) dimensionalities. Thus, microscopically different systems can be assembled into (d, n) universality classes, in which isomorphic/equivalent physical properties are described by the same values of critical exponents near critical (singular) points. This universal behavior splits into two categories: (i) non-classical, where the exponents are small irrational numbers, and (ii) classical ones, where the exponents are small integers or their ratios. The latter is associated with space dimensionalities $d \geq 4$ (single critical point, MF case), and $d \geq 3$ (the simplest multicritical point: TCP) [60–62]. The "classical" behavior is also linked to an "infinite" range of intermolecular/inter-element interactions at the microscopic level. One can recall the Ginzburg criterion [77,78] to comment on this issue and the interplay between classical and non-classical criticality. Applying the above discussion to the paraelectric–ferroelectric phase transition, one can relate the classical behavior to the following form of the criterion:

$$\frac{\langle \Delta P^2 \rangle}{P^2} = \frac{1}{\xi^d} \frac{kT\chi}{P^2} < 1, \tag{17}$$

where P has the meaning of the general order parameter and $\chi \propto |T - T_C|^{-\gamma}$ is the order-parameter-coupled susceptibility.

The Ginzburg criterion [77,78] shows that the classical–non-classical crossover can occur if the space-related range of interactions associated with pretransitional fluctuations becomes smaller than the range of microscopic "permanent" interactions (intermolecular, inter-element) characterizing a given system. This implies that for systems with non-classical critical behavior, the crossover to the classical one should occur far from the critical point, where the correlation length decreases enough. Indeed, such behavior has been evidenced, for instance, a few tens of Kelvin away from the critical consolute temperature in binary critical mixtures of limited miscibility ($d = 3$, $n = 1$ universality class: critical exponents $\gamma \approx 1.23$, $\beta \approx 0.325$, $\nu \approx 0.625$) [61,76]. However, in critical mixtures, the explicit classical behavior associated with exponents $\gamma = 1$, $\beta = 1/2$, $\nu \approx 1/2$ also has been demonstrated in the broad surroundings of T_C under the shear flow [79–83] or under the strong electric field [84,85], with the crossover to the non-classical behavior remote from T_C. It is a kind of "reversed criticality" under the exogenic uniaxial impact. The mentioned impacts cause the uniaxial elongation of precritical fluctuations, which is possible in the near-critical domain even under moderate external impacts [61]. In the given case, exogenic impacts do not affect intermolecular interactions, and the only factor leading to the "anomalous" appearance of classical behavior may be local uniaxial symmetry, which, in the given case, is induced by exogenic impacts. This concept led to the explanation of changes in the nonlinear dielectric effect (NDE) and the electro-optic Kerr effect (EKE) when approaching the critical consolute point and gas–liquid critical point [84,85]. It also became crucial in explaining the mean-field nature of NDE, EKE, and dielectric constant pretransitional changes in the isotropic liquid phase of nematogenic liquid crystals, where rod-like uniaxial symmetry is the inherent feature [84,85]. Recently, it was also used to show and explain the behavior of NDE, EKE, and the dielectric constant in the liquid phase on approaching the orientationally disordered crystal (ODIC) phase of plastic crystals [58].

For explaining such behavior, it is essential to understand the interrelation between the meaning of the increased dimensionality ($d \geq 4$, for MF case) and the "infinite" range of interactions. For both cases, it means that the number of nearest neighbors of a given molecule or element, related to the possibility of interactions ("visibility"), is greater than the number resulting from the simplest "geometrical packing" represented by spheres. This situation can occur when the local symmetry of the elements building the system is predominantly uniaxial. The above allows us to answer a fundamental question:

Why does the wide surrounding of the paraelectric–ferroelectric transition show the mean-field characterizations described by the Curie–Weiss "law" (Equation (1)), related to the MF exponent $\gamma = 1$?

In our opinion, it can be explained by the inherent uniaxiality, which is the origin of ferroelectricity and is associated with a uniaxial shift in charges within a basic element of the crystalline network.

As for the complex case of relaxor ferroelectric materials, one should take into account their basic material characterization, namely that they are composed of micrometric-size (l_{Grain}) grains, connected by "molten" surfaces, that can lead to partially amorphous inter-grain material. Consequently, it can be assumed that in the paraelectric phase of relaxor ceramics on cooling towards the para–ferro transition, first, the "canonical" ferroelectricity develops within grains until the correlation length approaches the grain size. According to the authors, this occurs at the temperature that can be associated with the Burns temperature, then $\xi(T_B) \sim l_G$. Further cooling towards the para-ferro transition cannot increase the correlation length of pre-ferroelectric fluctuations up to the infinite value (Equation (15a)), expected for classical, homogeneous ferroelectric systems. However, further cooling towards the transition can improve the pre-ferroelectric ordering within limited grain volumes. Consequently, one can expect the appearance of strong inter-grain local electric fields. They can lead to some coupling of fluctuations confined by grain borders, which can affect their interiors.

At this point, the temperature behavior of the order parameter under the coupled field is worth recalling. For ferromagnetic systems, it is the magnetization and the magnetic field; for ferroelectric systems, it is the electric polarization and the electric field. Under the permanent influence of such a (global or local) field, (electric or magnetic), the order parameter, instead of approaching zero to $T \to T_C$ according to Equation (12) shows a strong deviation when passing from the ferro- to the paraelectric phase. It preserves a non-zero value when passing from the high-temperature para- phase to the low-temperature ferro- phase, and vice versa. The onset and the value of this distortion depends on the field intensity. From Equations (11) and (14), the following relations can be obtained for the dielectric constant and the dielectric susceptibility.

$$\chi(T,P,E) = \varepsilon(T,P,E) - 1 = \left(\frac{\partial^2 F(T,P,E)}{\partial P^2}\right)^{-1} = \frac{1}{a + 3bP^2(E)} = \frac{1}{A(T-T_C) + 3bP^2(E)} = \frac{A^{-1}}{T - (T_C + 3A^{-1}bP^2(E))}. \quad (18)$$

The local electric field resulting from the ferroelectric arrangement within grains is not uniform in magnitude and direction. Following Equation (18), one can expect "pseudospinodal singular temperatures" [59,86] corresponding to different available maximum dielectric permittivity values.

It is noteworthy that parallel singular functional forms of pretransitional behavior should appear for Equations (1), (13), (14) and (18) on the approach to the "critical" temperature $T \to T_C$ and on the approach to the pseudospinodal temperature, $T \to T_{SP} = T_C + \left(3A^{-1}bP^2(E)\right)$ (Equation (18)). However, the latter is associated with finite terminal dielectric permittivity/dielectric constant values. For relaxor ceramics, the "generic" random local electric fields are self-induced on cooling towards the paraelectric–ferroelectric transitions, and the additional "frustration" (F) contribution can also be expected. It can affect the dielectric constant, the dielectric susceptibility, and the singular "critical-like temperature" $T_{SP} = T_C + \left(3A^{-1}bP^2(E) + F\right)$.

3.1.2. "Critical" View on Dynamics in Relaxor Systems

"Glassy" dynamics is the next unique feature of relaxor ceramics [1–52]. It is generally demonstrated by representing the evolution of the primary relaxation time with the VFT relation (Equations (3) and (4)), instead of the simple Arrhenius pattern $\tau(T) = \tau_\infty exp(E_a/RT)$ where $E_a = const$. Non-Debye changes in the shape of loss curves are often described using the HN relation (Equation (5)) [2,6–8,12–16,19,21–26,31–39,47]. Such a scaling pattern is also characteristic of the previtreous domain (i.e., above the glass temperature T_g) of glass-forming systems. The origin for these universalistic changes, related to $\tau(T_g) < 100s$ time-scales, remains a challenge [54–56]. For relaxor systems, they are explicitly related to the approach of the paraelectric–ferroelectric transition. The "glassy" dynamics can be associated with the development of the pretransitional fluctuation time-scale (Equation (15b)), which parallels a single-dipole-moment relaxation due to the MF nature of the phenomenon. Below T_B, which we associate with reaching the grain size limit via the correlation length of fluctuations (Equation (15a)), the increasing influence of the frustration associated with rising impacts of random internal local electric fields may appear. Interestingly, passing through T_B the Burns temperature does not affect the parameterization of $\tau(T)$ using the VFT relation [1–52].

Recently, it has been shown that the VFT relation is primarily an effective descriptive tool for glass-forming systems, and its fundamental importance is limited [56].

The insight based on the analysis of the apparent activation energy index $I_L(T) = -dlnE_a(T)/dlnT = (dE_a(T)/E_a(T))/(dT/T)$ led to the following expression for configurational entropy changes [56,87]:

$$S_C(T) = S_0 t^n = S_0 \left(\frac{T - T_K}{T}\right)^n = S_0 \left(1 - \frac{T_K}{T}\right)^n, \tag{19a}$$

$$lnS_C(T) = lnS_0 + nlnt \Rightarrow \left(\frac{dlnS_C(T)}{d(1/T)}\right)^{-1} = \left(\frac{1}{nT_K}\right) + n^{-1}T^{-1}, \tag{19b}$$

where $S_0 = const$, T_K is related to the so-called Kauzmann temperature, the exponent $0.18 < n < 1.6$; the upper limit is related to the dominance of the orientational local ordering (naturally coupled to uniaxiality), and the lower one to the translational order. For $n = 1$, a system has no preferable type of the local symmetry.

This leads to the following "VFT-extended" equation [56,87–89]:

$$\tau(T) = \tau_\infty exp\left(\frac{D}{T} t^{-n}\right) = \tau_\infty exp\left(\frac{DT^{n-1}}{(T - T_K)^n}\right). \tag{20}$$

This relation correlates with the VFT equation for $n = 1$, but the analysis of experimental data shows that for relaxor systems $n > 1$ [56,87–89]. However, the "generalized VFT" Equation (20) contains four fitting parameters, significantly reducing the analysis's reliability. Obtaining the n parameter independently may be a solution, for example, using the configurational entropy analysis, as defined by Equation (19b). However, it requires high-resolution and long-range experimental results of the heat capacity measurements to determine changes in configurational entropy, which are rarely available.

Recently, a new universalistic description of the so-called steepness index has been shown: $m_T(T) = dlog_{10}\tau(T)/d(T_g/T)$. Note that it is proportional to the apparent activation enthalpy $H_a(T) = dln\tau(T)/d(1/T)$ [90]:

$$m_T(T) = \frac{dlog_{10}\tau(T)}{d(T_g/T)} = \frac{1}{T_g ln10}\frac{dln\tau(T)}{d(1/T)} = C \times H_a(T) = C\frac{M}{T - T_g^*}, \tag{21}$$

where $C, M = const$ and $T_g^* < T_g$ is the extrapolated singular glass (vitrification) temperature.

The above relation directly leads to the following three-parameter dependence for the primary relaxation time [90]:

$$\tau(T) = C_\Gamma \left(t^{-1} exp(t)\right)^\Gamma, \tag{22a}$$

$$ln\tau(T) = lnC_\Gamma + \Gamma(t - lnt), \tag{22b}$$

where $t = \left(T - T_g^*\right)/T$ and $C_\Gamma = const$.

The number of adjustable parameters can be reduced to only two, since T_g^* can be easily determined via scaling Equation (21), using the linear regression for the experimental data presented in the plot $H_a^{-1} = (dln\tau(T)/d(1/T))^{-1}$ vs. T. Knowing T_g^*, one can present the experimental data using the plot defined by Equation (22b), namely $ln\tau(T)$ vs. $t - lnt$. We can then use the linear regression fit, and one can estimate the optimal values of C_Γ and Γ parameters. Thus, the nonlinear fitting can be totally avoided for portraying $\tau(T)$ changes via Equation (22a).

Equation (22) relates characteristics of the "activated" (i.e., SA-type: Equation (3a)) and the critical-like behavior. It is notable that there is a link between the exponent Γ and the dominant local symmetry in the given system.

If the uniaxial or translational symmetries are dominant, Equation (22a) can be fairly approximated by an even more straightforward critical-like relation [56,90,91]:

$$\tau(T) = \tau_0 (T - T_C^*)^\varphi, \tag{23}$$

where the exponent $\varphi \approx 9$ and $T_C^* < T_g$.

In particular, Equation (23) correlates with the so-called dynamical scaling model (DSM) [92], whose check-point is related to the exponent $\varphi = 9$. It was suggested to be "universal", at least for glass forming low-molecular-weight liquids and polymers [92]. Such a statement has not found a reliable experimental confirmation [56]. However, the authors of this work (ADR, SJR) have shown, using a distortions-sensitive analysis, that Equation (23) perfectly describes liquid crystalline (LC) systems, with the inherent uniaxial symmetry of molecules. We emphasize this fact because DSM is the "generic" mean-field model. The classical MF/TCP characterization is also the generic feature of the mentioned rod-like LC systems due to their local uniaxiality [56,90,91].

The discussion presented in this section suggests that the standard VFT relation used to describe "glassy dynamics" in relaxor systems should be considered as an effective tool with limited fundamental significance. The role of the critical-like, mean-field description and the importance of uniaxial symmetry seems to be crucial. It correlates with the discussion of static properties, namely dielectric susceptibility and dielectric constant in Section 3.1.1.

3.1.3. "Critical" View on Clausius–Mossotti Local Field in Ferroelectric Systems

Shortly after Michel Faraday introduced the dielectric constant to characterize the properties of dielectrics, this quantity became important for gaining fundamental insight into the microscopic properties of this type of materials [93]. In 1850, Ottaviano Mossotti proposed the first local field model concept [94]. After supplementations introduced by Rudolf Clausius, it is called the Clausius–Mossotti local field model [95,96]. Further developments of this concept considered a molecule/element inside a cavity in a dielectric, under an external electric field E [95,96]:

$$F = E + E_1 + E_2, \tag{24}$$

where E_2 is the electric field created by elements/molecules within a semi-microscopic cavity surrounding a given molecule/element, and E_1 results from charges situated on the surface of the cavity.

For a dielectric system (basically gas or liquid) with a random distribution of elements or a regular crystalline lattice (for solids), $E_2 = 0$. In such a case, summarizing the effect of the cavity surface charge, one obtains [95,96]:

$$E_1 = P/3\varepsilon_0, \tag{25}$$

where P denotes the polarization vector and $\varepsilon_0 = 8.854\ (pFm^{-1})$ is the vacuum electric permittivity.

This approximation can be applied to gaseous dielectrics with non-interacting molecules or non-dipolar liquids [95,96]. Let us recall the dielectric displacement vector: $D = \varepsilon_0 E + P = (\chi' + 1)\varepsilon_0 E = \varepsilon_0 \varepsilon' E$ and the relation between the polarizability vector and the basic element/molecule polarization: $P = \varepsilon_0 \chi' E = N\alpha_p F$, where α means the basic element/molecule polarizability and $N = N_A M^{-1}$ stands for the number of base elements/molecules per unit volume, ρ is density, M is the molecular mass, and N_A is the Avogadro number. Taking this into account, Equation (24) and the fact that $E_2 = 0$, one obtains [95,96]:

$$F = \frac{P}{3\varepsilon_0} = \frac{\chi'}{\chi' + 3} P \Rightarrow \quad \chi' = \frac{N\alpha_P}{3\varepsilon_0} \frac{\chi'}{\chi' + 3}. \tag{26}$$

The re-arrangement of the latter yields:

$$\chi' = \frac{P}{\varepsilon_o E} = \frac{N\alpha_P/\varepsilon_0}{1 - N\alpha_P/3\varepsilon_0}. \tag{27}$$

The above relations (Equations (24)–(27)) show canonic results presented in classic monographs on dielectrics physics [95,96]. Von Hippel [95] supplemented Equation (27) by considering dipolar dielectrics, especially liquid ones, and using the relation introduced by Debye $\alpha_P = \mu^2/3k_B T$. It transformed Equation (27) into the following form [95,96]:

$$\chi = \varepsilon - 1 = \frac{3T_C}{1 - T_C}, \tag{28}$$

where $T_C = N\mu^2/9k_B\varepsilon_0$.

In his classic monograph [95], von Hippel pointed out the paradoxical consequences of this reasoning for such a common dipolar dielectric liquid as water. He pointed out that it leads to the paraelectric–ferroelectric transition at $T_C \approx 1520$ K, and concluded [95]: "water should solidify by spontaneous polarization at high temperature, making life impossible on this earth!" This paradoxical result is often cited in monographs and presented in undergraduate lectures for students due to its impressiveness and to show the consequences of violating the basic assumptions of a given model. Von Hippel associated the paradox with the lack of short-range interactions associated with the non-zero field E_2. The paradox anomaly for dielectric liquids has been removed by the inclusion of short-range interactions, for example in Kirkwood or Froelich models, commonly used to interpret experimental data for decades [96]. It should be noted that von Hippel's paradox example ignores an important fact. He considered the density of water for "normal" conditions, i.e., d = 1 g/cm^3 [95,96]. However, for $T > T_C \approx 1520$ K such density is only possible under multi-GPa pressures. It can even lead to exotic properties often detected for materials at extreme pressures.

The following summary from the monograph *Dielectric Physics* by Chełkowski can summarize the considerations regarding the application of the Clausius–Mossotti local field model [96]: "(. . .) it is obvious that in the case of dipolar materials (. . .) the Lorentz field model cannot be employed".

However, there are materials for which the Clausius–Mossotti model can be applied. These are the solid phase of classical ferroelectrics or liquid crystalline ferroelectrics. Both systems are inherently associated with significant permanent dipole moments. Several models deal with this topic [63–68] and refs. therein, essentially referring to the qualitative explanation of von Hippel [96], who stated that in ferroelectric materials, an applied electric field or thermal motion can induce a charge displacement and, hence, a net dipole moment within the crystalline network, which can be further increased by the additional displacement caused by inter-ion couplings. The process continues until the thermal motion is overcome at a critical temperature.

But the question remains: Why is the Clausius–Mossotti local field model obeyed in ferroelectric materials? According to the authors, the key argument in favor of such

behavior is tautological: it recalls the similarity between the Curie–Weiss and the Mossotti Catastrophe equations, i.e., Equations (1) and (28).

The "Critical" discussion in Sections 3.1.1 and 3.1.2 can provide an answer. The intrinsic link between the basic mechanism of the appearance of ferroelectricity and the uniaxial symmetry leads to the mean-field characterization. It implies the "immersion" of induced dipole moments in the mean-field surrounding. As a result, a kind of "effective gas" of independent dipole moments can appear, which correlates with the basic assumption of the Clausius–Mossotti local field model. Deviations from this picture can be associated with the emergence of additional specific material properties, e.g., in the broad surroundings of the paraelectric–ferroelectric transition for relaxor ceramics.

3.2. Experimental Results and Discussion

The studies were carried out in a $Ba_{0.65}Sr_{0.35}TiO_3$ relaxor ceramic (99.3%). Its preparation and characterization are described in the Methods section. It also includes frequency-related ($T = const$. Figure 3) and temperature-related ($f = const$: Figure 4) master plots showing the real and imaginary components of the complex dielectric permittivity: see also Appendix A for the complete data set. The results presented in the Methods section were selected from data covering 250 tested temperatures in the range 123 K $< T <$ 373 K, to illustrate general features. The dielectric constant is the basic property whose temperature evolution is considered for relaxor ceramics. However, the canonical definition of the dielectric constant in Dielectrics Physics [95,96] defines it as the nearly constant value of $\varepsilon' = \varepsilon$ in the static frequency domain, where a frequency shift has a negligible effect on the measured values. It is visualized as the horizontal domain in $\varepsilon'(f, T = const)$ spectrum. For dipolar dielectrics, it usually occurs for 1 kHz $< f <$ 10 MHz [55,58,95,96].

The results presented in Appendix A show that such behavior is almost absent for the tested relaxor ceramics, especially near the paraelectric–ferroelectric transition. The static-type horizontal behavior appears only well above the transition (for the isotherm $T = 373$ K) and for $T \approx 200$ K $\pm$ 30. It is noteworthy that the Curie–Weiss temperature $T_C \approx 292$ K.

Consequently, the Curie–Weiss behavior for relaxor ceramics should be discussed in frames of the real part of dielectric permittivity, and the "dielectric constant" should be treated as the replacement name and written "in parentheses", in the opinion of the authors. For this meaning of "dielectric constant", the frequency $f = 10$ kHz can be a reasonable choice for the tested system.

Figures 5–7 show different aspects of $\varepsilon'(T, f = 10$ kHz$)$, focused on testing the temperature evolution via a distortions-sensitive and derivative-based analysis (Figure 6) [56,58,90,91,97]. Such an analysis has already been applied in glass-forming systems and "critical" liquids, revealing significant features that are hidden for the direct nonlinear fitting of experimental data [56].

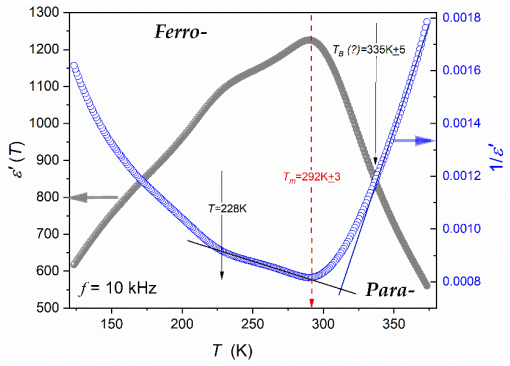

Figure 5. Temperature changes in the real part of dielectric permittivity, related to the so-called "dielectric constant" and its reciprocal. Results for $Ba_{0.65}Sr_{0.35}TiO_3$ relaxor ceramic. The Burns temperature T_B is indicated. According to this report, T_B is not a significant material characteristic, which is expressed with a "?".

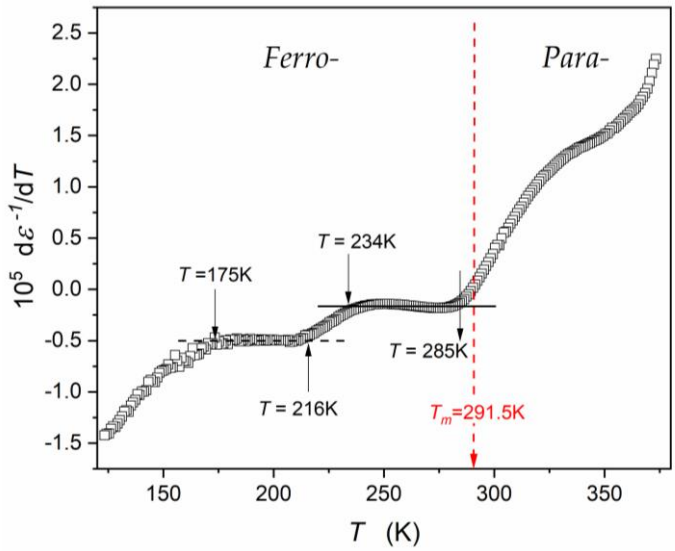

Figure 6. Temperature changes in "the dielectric constant" reciprocal derivative, focused on the distortions-sensitive test of the Curie–Weiss behavior, manifesting via horizontal lines. The analysis for $Ba_{0.65}Sr_{0.35}TiO_3$ relaxor ceramic-based on experimental data is shown in Figure 5.

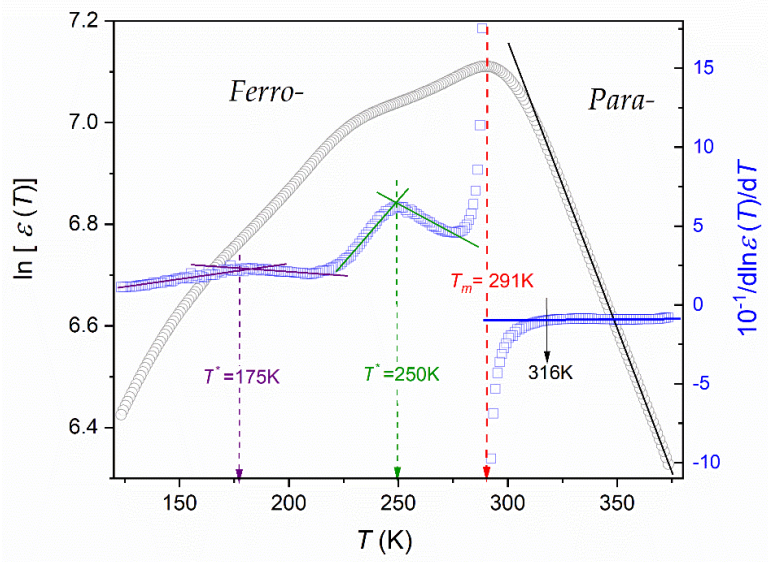

Figure 7. Temperature changes in the logarithm of the "dielectric constant" and the reciprocal of its derivative for the distortions-sensitive test of such behavior, which is manifested by the horizontal line. The analysis for $Ba_{0.65}Sr_{0.35}TiO_3$ relaxor ceramic is based on experimental data from Figure 5.

Figure 5 presents the temperature evolution of the "dielectric constant" in the temperature range covering 250 K, including the evolution of its reciprocal. The latter is reminiscent of the commonly used analysis, focused on the Curie–Weiss relation (Equation (1)). It is also used to determine the Burns temperature T_B, which is related to the distortion from CW behavior when approaching the paraelectric–ferroelectric transition. The departure from CW Equation (1) is gradual, and precise estimation of its value is not possible, namely: $T_B = 340\ \mathrm{K} \pm 5\ \mathrm{K}$. Linear changes of $1/\varepsilon(T)$ in the paraelectric phase can be considered as a confirmation of the process description via the Curie–Weiss Equation (1). It covers the temperature range of about 50 K, although a weak bias appears when approaching the high temperature limit ($T \approx 375$ K).

The precise determination of the T_B value and the validation of the CW description offers a distortions-sensitive data analysis recalling Equation (1b):

$$\frac{d(1/\varepsilon(T))}{dT} = \frac{d\left(A_{CW}^{-1}T - A_{CW}^{-1}T_C\right)}{dT} = A_{CW}^{-1} = const., \quad (29)$$

Such an analysis is shown in Figure 6: the horizontal line, expected according to Equation (29), appears only on the ferroelectric side of the curve related to the paraelectric–ferroelectric transition. There is no horizontal line on the paraelectric side where studies in relaxor systems are focused. Hence, the result validating the Curie–Weiss-type description in the paraelectric phase is negative.

In particular, in the ferroelectric phase, near $T \approx 170$ K, a feature of the next phase transition appears. For $T > 170$ K, it follows the pattern parallel to Equation (29), for ca. 40 K.

Figure 7 shows the experimental data from Figure 5 using the semi-log scale. The distortions-sensitive and derivative-based analysis complements the results. It has two aims. The first is to confirm the (surprising) fairly exponential behavior covering the range between $T \sim 375$ K and $T \sim 315$ K:

$$\varepsilon(T) = \varepsilon_{ref.} exp(a\prime T) \Rightarrow ln\varepsilon(T) = ln\varepsilon_{ref.} + a\prime T, \quad (30)$$

where $\varepsilon_{ref.}, a' = const.$

Such behavior is validated by the solid line in Figure 7. It is supplemented by the distortions-sensitive and derivative-based analysis, presented as $[dln\varepsilon(T)/dT]^{-1}$ vs. T analytic plot. It enables the "subtle" test of the existence of critical-like domains, described as follows:

$$\varepsilon(T) = \varepsilon^0\left|T - T^*\right|^{-\Phi} \Rightarrow ln\varepsilon(T) = ln\varepsilon^0 - \phi ln\left|T - T^*\right| \Rightarrow \frac{d(ln\varepsilon(T))}{dT} = \frac{-\phi}{|T - T^*|} \Rightarrow \left[\frac{d(ln\varepsilon(T))}{dT}\right]^{-1} = -\phi T \mp \phi T^* = a + bT, \quad (31)$$

where $\varepsilon^0, a, b = const$, T^* stands for the critical-like temperature and ϕ is the "critical" exponent.

The above plot also allows the validation of Equation (30), which gives a horizontal line, namely:

$$\left[\frac{d(ln\varepsilon(T))}{dT}\right]^{-1} = \left(a'\right)^{-1} = const.. \quad (32)$$

Thus, Equation (30) provides an optimal representation of the experimental data in the paraelectric phase. There is a remarkable agreement between Equation (30) and the output model-relations (Equation (9)), proposed in ref. [7].

Figure 7 also presents the results of the derivative-based analysis of "the dielectric constant" changes in the surrounding of its maximum, associated with the transition from the paraelectric to the ferroelectric phase.

The linear domain detected in such analysis is related to (Figure 8):

$$\frac{d(ln\varepsilon(T))}{dT} = a + bT \Rightarrow d(ln\varepsilon(T)) = (a + bT)dT. \quad (33)$$

The integration of the above yields:

$$\varepsilon(T) = A\exp\left(c + aT + bT^2\right) \text{ for } 285 \text{ K} < T < 314 \text{ K}, \quad (34)$$

i.e., for the surroundings of the paraelectric–ferroelectric transition.

For the paraelectric side of the transition, the following portrayal was validated (Figure 7):

$$\varepsilon(T) = A\exp(b + aT) \text{ for } 315 \text{ K} < T < 375 \text{ K}, \quad (35)$$

while for the ferroelectric side of the transition:

$$\varepsilon(T) = \frac{C}{|T - T_C|} \text{ for } 234 \text{ K} < T < 285 \text{ K}, \quad (36)$$

i.e., correlated with the mean-field Landau–Devonshire model [74,75].

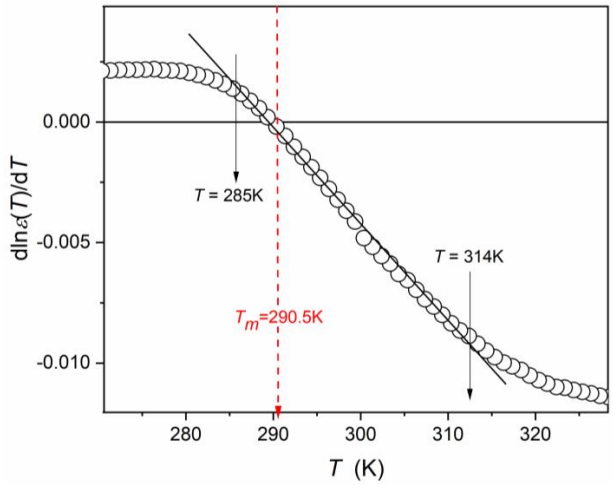

Figure 8. Temperature changes in the derivative of "dielectric constant" ($\varepsilon'(f = 10$ kHz)) logarithm in the surroundings of the paraelectric–ferroelectric transition. The dashed red line indicates the temperature of the "dielectric constant" maximal value. Solid, black arrows indicate terminals of the linear behavior. The analysis for $Ba_{0.65}Sr_{0.35}TiO_3$ relaxor ceramic based on experimental data shown in Figure 5.

In particular, there are almost no "gaps" between the descriptions related to the following temperature domains.

Temperature changes in the imaginary part of the dielectric permittivity for the discussed "quasi-static" frequency $f = 10$ kHz are shown in Figure 9. This magnitude reflects the energy absorbed for subsequent processes, complementing the message from the scan of the real component, which mainly reflects the appearance and arrangement of permanent dipole moments [58,96]. In the ferroelectric phase, there is a strong manifestation of relaxation processes, which, for $\varepsilon'(T)$ only become explicitly visible only for disturbances-sensitive and derivative-based analysis. This evidence is even stronger, especially in the paraelectric phase, for the dielectric loss tangent $tan\delta = \varepsilon''/\varepsilon'$, which can be related to the fact that this quantity $D = tan\delta =$ (energy lost per cycle/energy stored per cycle).

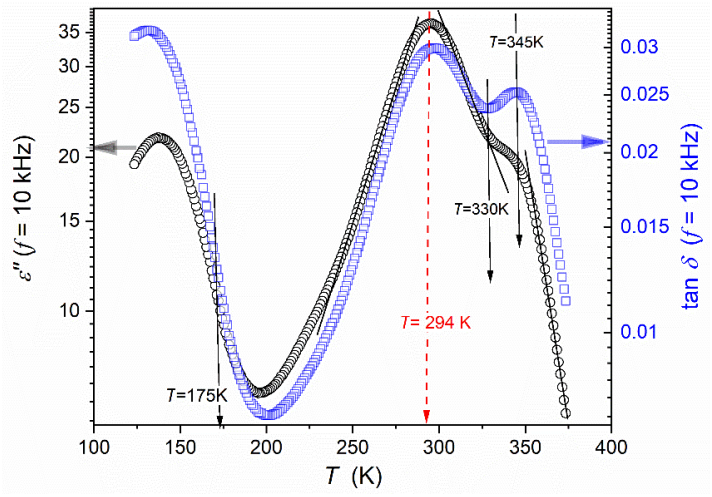

Figure 9. Temperature changes of the imaginary part of dielectric permittivity ($\varepsilon''(f = 10$ kHz)) and related $\tan\varepsilon = \varepsilon''/\varepsilon'$. The solid, black line indicates characteristic temperatures, and the dashed red line is related to the paraelectric–ferroelectric transition: note a slight shift in comparison with temperatures detected in $\varepsilon'(T)$ analysis. The results are for $Ba_{0.65}Sr_{0.35}TiO_3$ relaxor ceramic (see Figure 3 and Appendix A).

In Figure 9, the cycle is related to $f = 10$ kHz, i.e., it determines the energy of the process itself, minimizing the influence of the "background", related to the "whole" system [58,95,96]. This property is also called the dissipation factor, and it is used to define the quality factor $Q = 1/D$, significant for applications in materials engineering.

Figure 9 shows that the tested system is characterized by a relatively low dissipation/loss factor. It increases on approaching the paraelectric–ferroelectric transition, which can be related to an increasing number of permanent dipole moments and ability to interact with the external electric field and is also coupled within multi-element fluctuations. The latter are associated with the anomalously increasing susceptibility $\chi = \varepsilon - 1$ reflecting the increasing sensitivity of local order parameter changes (polarizability) to the electric field. This effect diminishes away from the transition. The impact on $tan\delta(T)$ evolution is shown in Figure 10.

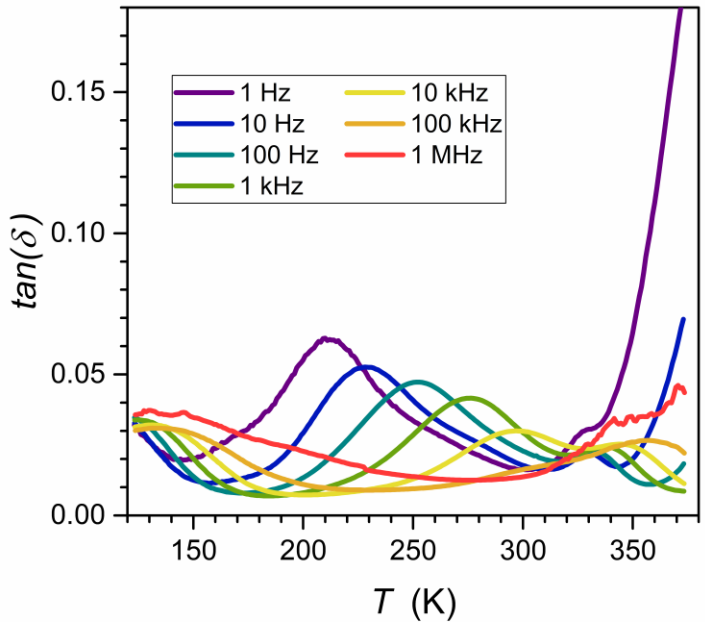

Figure 10. Temperature evolutions of $tg\ (T, f = const) = \varepsilon''(f,T)/\varepsilon'(f,T)$ for selected frequencies in the tested relaxor ceramic, specified in Table 1.

Relaxation times appearing in dielectric permittivity spectra were determined from peak frequencies of loss curves $\tau = 1/2\pi f_{peak}$, supported by the analysis of $dlog_{10}\varepsilon''(T)/dT$ and $dlog_{10}\varepsilon''(f)/dlog_{10}f$ allowing its unambiguous estimation. This protocol avoids the significant uncertainty for the determination of relaxation times via the Havriliak–Negami relation [58], which requires nonlinear fitting. Such fitting is associated with at least four adjustable parameters, and their number increases to eight when the merging of two relaxation processes creates the loss curve. Loss curves for characteristic temperature ranges, with indications of basic relaxation processes and coupled relaxation times, are shown in Figure 11.

Figure 12 presents the map of relaxation times using the Arrhenius scale: $log_{10}\tau(T)$ vs. $1/T$. The inset shows the relaxation time τ_3 at low temperatures in the ferroelectric state. It appears that the tested system exhibits a unique feature. Usually, the super-Arrhenius behavior occurs in the paraelectric phase and terminates close to T_m. For the tested compound it terminates at $T_{term.} \approx 330$ K, considering $\tau_1(1/T)$ changes. The super-Arrhenius (SA) behavior of $\tau_2(1/T)$ behavior is notable. The SA behavior is related to Equation (22) and has been shown by the apparent activation enthalpy tests, which focused on validating the SA behavior representation by Equation (21). This result is shown in Figure 13. On further cooling towards the transition, a new process emerges. It explicitly follows the simple Arrhenius pattern, with the constant activation energy extending deeply into the ferroelectric state,

with no hallmark when passing T_m temperature (Figure 12). The height (maximum) of the associated loss curves increases strongly on cooling, as shown in Figure 14. Figure 15 presents the scaled superposition of loss curves related to τ_2 relaxation time, showing the essentially non-Debye and broad distribution of relaxation times.

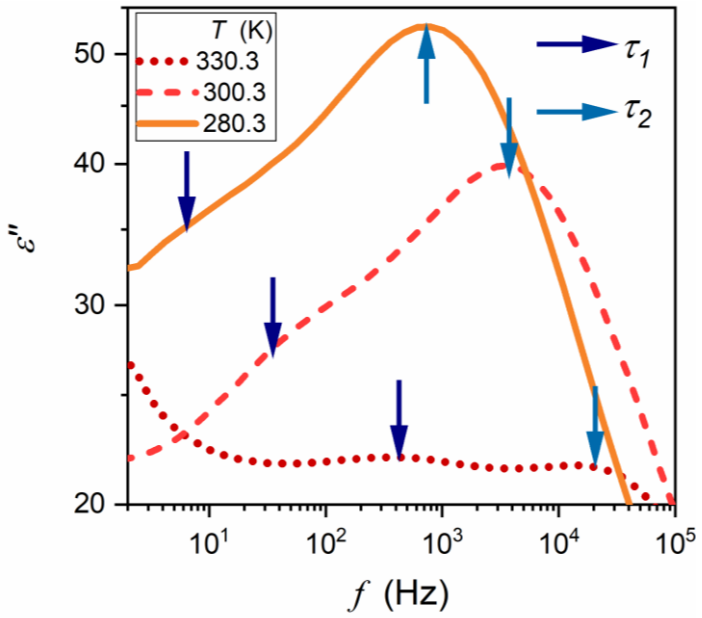

Figure 11. Dielectric loss curves at three selected temperatures in the para- and ferroelectric phases. Relevant relaxation processes are indicated. Results are for $Ba_{0.65}Sr_{0.35}TiO_3$ relaxor ceramic.

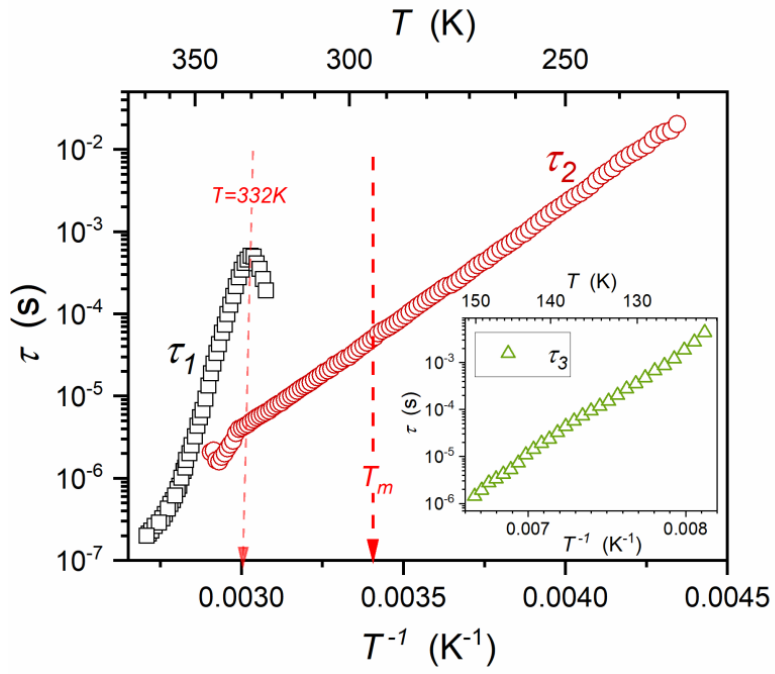

Figure 12. Arrhenius plot of relaxation times detected in $Ba_{0.65}Sr_{0.35}TiO_3$ relaxor ceramics. The inset shows changes in relaxation time of the process emerging in the ferroelectric phase at low temperatures.

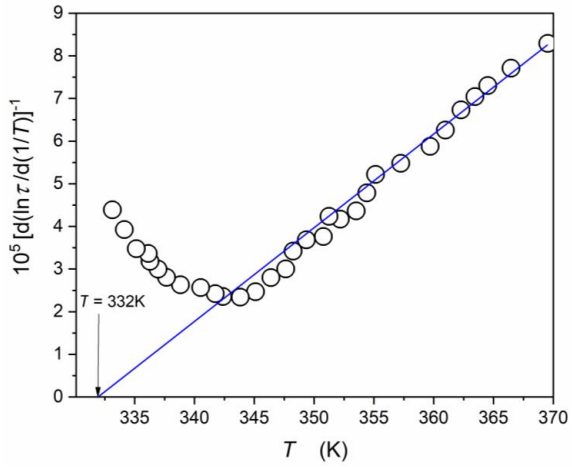

Figure 13. The temperature dependence of the reciprocal of the apparent activation enthalpy focused on validating Equations (21) and (22), which should manifest as linear behavior. The singular temperature T^* is indicated by the arrow.

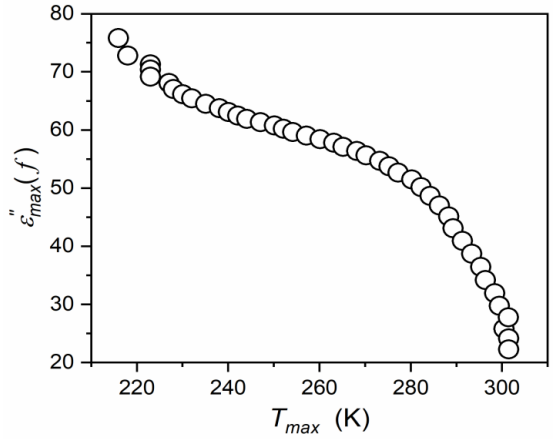

Figure 14. Temperature changes of the maxima of loss curves related to ε_2 relaxation time, as indicated in Figure 12.

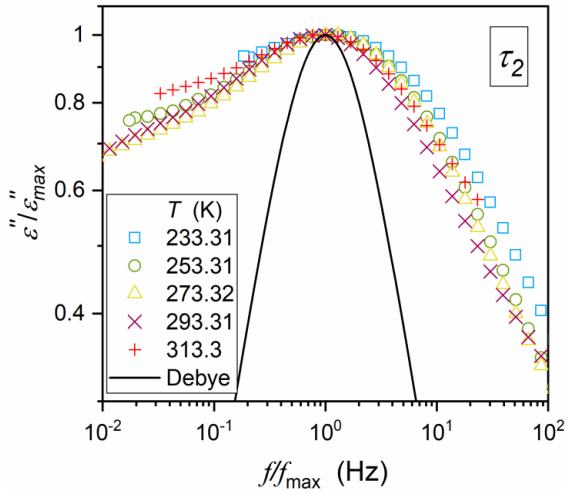

Figure 15. Time–temperature–superposition (TTS) of relaxation time in the tested relaxor ceramic, covering both paraelectric and ferroelectric phases. For comparison, the single relaxation time-related Debye distribution is also shown. The plot is presented in the log-log scale.

In the ferroelectric phase, phase transformations were detected, as can be seen for temperature evolution of "the dielectric constant" (Figure 7), which suggests a link with the arrangement of permanent dipole moments, and also for $\varepsilon''(T)$ and $tan\delta(T)$, which may reflect the energy loss associated with these phenomena. The process related to the lowest temperature introduces an additional relaxation time τ_3. Its temperature evolution follows the basic Arrhenius pattern, as it is shown in the inset in Figure 12.

For applications of relaxor systems, the sensitivity of the dielectric properties, in particular the "dielectric constant", to the external electric field is essential. The fundamental origins of such behavior in relaxor ceramics also have remained a challenge. Figure 16 shows such behavior for the relaxor ceramic discussed in the report. Figure 17 presents the same experimental data, but in respect to the reference at ($U = 0$, $E = 0$): $\Delta\varepsilon(E) = \varepsilon(E = 0) - \varepsilon(E)$, i.e., relative changes in "the dielectric constant". In particular, relatively large changes in "the dielectric constant" occur for relatively weak electric fields in the tested material.

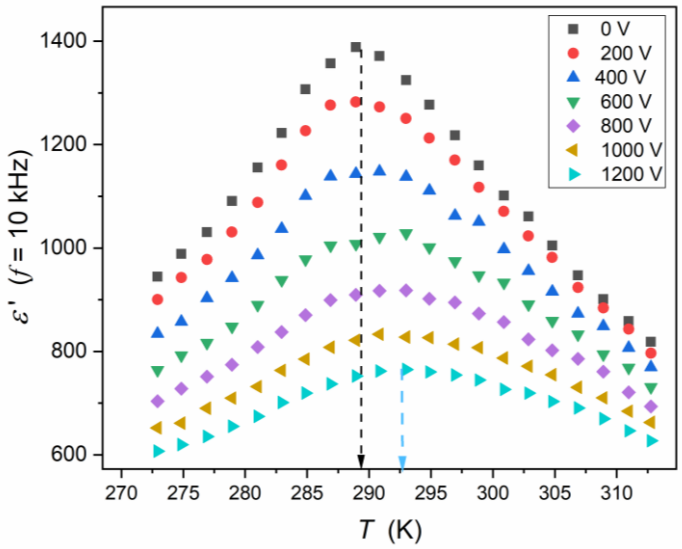

Figure 16. Changes in "dielectric constant" ($f = 10$ kHz) for $Ba_{0.65}Sr_{0.35}TiO_3$ sample, specified in Table 1. The sample was in the form of a disc of height $h = 1$ mm. Measurement voltages are given in the figure. The arrows indicate maximal values.

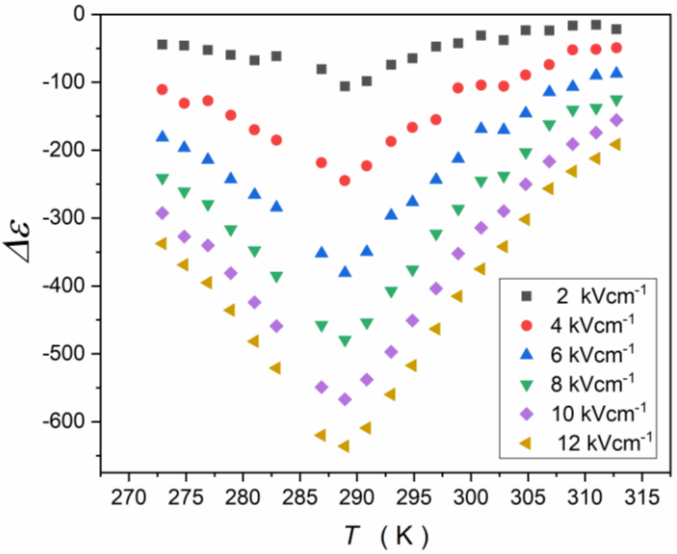

Figure 17. Relative changes in "dielectric constant" ($f = 10$ kHz) for $Ba_{0.65}Sr_{0.35}TiO_3$ sample (specified in Table 1). Scans collected under electric field $E \neq 0$ are compared to $E = 0$ behavior.

It is also worth noting that a relatively large shift in the $\varepsilon(T)$ curve maximum reaching $\Delta T(E) \approx 3$ K for the electric field $E = 12$ kVcm^{-1}. This shows the notable manifestation of the electrocaloric effect [49] in the given system.

Figure 18 presents the test of the electric field intensity, or the applied voltage, impact on $\Delta\varepsilon(E) = \varepsilon(E = 0) - \varepsilon(E)$, in the vicinity of the paraelectric–ferroelectric transition. The red curves show that the following polynomial can describe experimental data:

$$\Delta\varepsilon(E) = \varepsilon_{ref.} + aE^2 + bE^4, \tag{37}$$

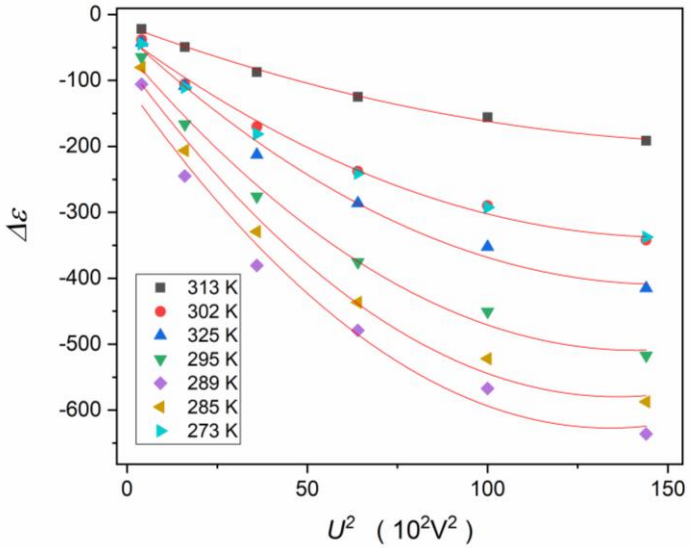

Figure 18. Relative changes in "dielectric constant" ($f = 10$ kHz) in $Ba_{0.65}Sr_{0.35}TiO_3$ sample (specified in Table 1), versus the square of the applied voltage to $h = 1$ mm "thick" sample.

This report shows that it is possible to describe the temperature changes in the dielectric constant for the following domains: (i) in the ferroelectric phase (Equation (36)); (ii) in the vicinity of the diffused, temperature-stretched, paraelectric–ferroelectric transition (Equation (34)); and (iii) in the paraelectric phase (Equation (35)). The transition to the subsequent domains occurs without a significant temperature gap, which allows us to consider the tunability characterization (Equation (2)), i.e., the relative changes in the "dielectric constant" caused by an external electric field [9,12,14–16,24,25,27,28,34–36]:

$$T = \frac{\varepsilon(E \to 0) - \varepsilon(E)}{\varepsilon(E \to 0)} = 1 - \frac{\varepsilon(E)}{\varepsilon(E \to 0)}. \tag{38}$$

For the ferroelectric side of the para-ferro transition, where the CW Equation (1) is obeyed, one obtains:

$$T = 1 - \frac{A_{CW}(E)}{A_{CW}} \frac{T - T_C}{T - T_C(E)}. \tag{39}$$

It reduces to the temperature-independent parameter $T = 1 - A_{CW}(E)/A_{CW}$ if the $T_C(E)$ shift is negligible.

For the paraelectric side of the transition, related to Equation (35), one obtains:

$$T = 1 - \frac{A}{A(E)} exp(\Delta b - \Delta aT), \tag{40}$$

where $\Delta a = a(E) - a$ and $\Delta b = b(E) - b$, where a and b are related to $E = 0$.

For the "diffused" surrounding of the para-ferro transition, one obtains:

$$T = 1 - \frac{A}{A(E)} exp\left(\Delta b - \Delta aT - \Delta cT^2\right). \tag{41}$$

3.3. Summary of Results

1. First, a new model for understanding and explaining the *physics of relaxor ceramics* is presented. It is based on references to the fundamentals of *Critical Phenomena Physics* and *Glass Transition Physics*. A particularly notable feature is the focus on the role of local symmetry, in this case uniaxial, which is particularly focused. The proposed model combines the unique properties of ceramic relaxors with the formation of random local electric fields resulting from pretransitional ferroelectric fluctuations inside ceramic "grains", i.e., confined by grain boundaries. Local electric fields create a specific feedback mechanism that couples the grain-constrained ferroelectric domains and also affect the interior of the grain-constrained ferroelectric domains, causing a bias towards the discontinuous transition. This gives rise to a singular pseudospinodal behavior [89], similar to the critical one, but is associated with an inherent non-zero order parameter (polarization in this case). Another notable feature of the model is the inherent link to basic experimental features. These are characteristic temperature changes in the "dielectric constant", electric-field-related stability, and glassy dynamics. The latter relates to the natural introduction of non-Arrhenius temperature variations and extreme non-Debye broadening of the primary loss curves.

The model highlights an additional fundamental feature of relaxor ceramics that has been overlooked so far. This is the absence of the "canonic" dielectric constant, defined in *Dielectrics Physics* as the "horizontal" and frequency-independent domain of the real part of the dielectric permittivity spectrum. Therefore, for relaxor ceramics, one should consider the real part of the dielectric permittivity for a selected frequency, and the name "dielectric constant" should be used in quotation marks.

2. The second part of the report presents the experimental results. They are based on relaxor ceramics specially prepared for this work. The innovative differential analysis for the temperature evolution of "dielectric constant" was used. An important result is an explicit demonstration that the "dielectric constant" in the paraelectric phase prefers not the Curie–Weiss portrayal but the exponential description. The results also challenge the "omnipotence" of the VFT relation as the "proof" for the glassy dynamics.
3. Based on the results discussed in points (1) and (2), it was possible to describe in a new way the full range of temperature changes of the "dielectric constant" in the para- and ferroelectric phases, for the "diffused" top-domain, and in the ferroelectric phase, virtually without gaps between domains. Equations describing the temperature dependences of the electric-field-related tunability have also been proposed.

4. Conclusions

This report presents a model discussion of the unique properties of relaxor ceramics in relation to Critical Phenomena Physics [59–62], Glass Transition Physics [54–56], and the reference to basic "homogeneous" ferroelectrics.

It indicates the importance of pretransitional fluctuations and the importance of uniaxiality in creating mean-field conditions near the paraelectric–ferroelectric transition, in both "homogeneous" and "heterogeneous" (i.e., relaxor ceramics) materials. The discussion includes the extended Devonshire–Landau model [72,73] and some new conclusions for the Clausius–Mossotti [94–96] local field model.

It is proposed that random local electric fields between ceramic grains with pre-ferroelectric arrangement, caused by pretransitional fluctuations, are responsible for the generation of characteristic $\varepsilon(T)$ changes in relaxor ceramics in the broad vicinity of the paraelectric–ferroelectric transition. The action of such local electric fields results in a distribution of local "Curie–Weiss type" domains, associated with a set of pseudospinodal [89] singular temperatures coupled to weakly discontinuous phase transitions:

$$\varepsilon(T) = \frac{A_{Sp}^{local}}{T - T_{Sp}^{local}(E)}. \quad (42)$$

Pseudospinodal behavior leads to finite $\varepsilon(T)$ "terminate" values because the discontinuous transition occurs before reaching the singular temperature T_{Sp}. It is noteworthy that such a picture allows to avoid problems of the essentially heuristic concept of local critical temperatures T_C (Equation (1)) resulting from PNR fluctuations, causing local concentration changes, often recalled in the modeling of relaxor ceramics properties [2–54].

In particular, for basic, "homogeneous", ferroelectric materials, even a strong external electric field initially leads to non-linear changes in the dielectric constant, which are described by so-called gap-exponents [98]. For relaxor ceramics, a moderate external electric field is already sufficient to strongly decrease the dielectric constant (ε') leading to tunability, which is crucial for applications. The given concept can be associated with the possibility of relatively easy interaction between intergranular electric fields and the external field.

In simple "homogeneous" ferroelectric materials, the static domain manifested via "horizontal changes" in $\varepsilon'(f, T = const)$ scan within the frequency range 1 kHz $< f <$ 10 MHz is the common feature. In a static domain $\varepsilon'(f) \approx \varepsilon = const$, despite a frequency shift. This is also the definition of the canonical dielectric constant. For relaxor ceramics, this behavior is absent, and some frequency change of $\varepsilon'(f)$ in the above frequency range is a standard feature. This is shown, for example, in Figure 3 and in Figure A1 in Appendix A. It can also be inferred from numerous reports on relaxor ceramics. In the opinion of the authors, the frequency-dependent "quasi-dielectric constant" is the next hallmark of relaxor ceramics. Such behavior can be deduced from the conceptual model proposed in the report.

For the conceptual model presented, the spatial growth of pretransitional/pre-ferroelectric fluctuations can be estimated by the counterpart of Equation (15a):

$$\xi(T) = \xi_0 \left| T - T_{Sp}(E) \right|^{-\nu}. \quad (43)$$

This pseudospinodal [60,89] correlation length is limited by the grain size, i.e., $\xi(T) < l_{grain}$ and additionally influenced by the impact of local electric fields on the singular temperature $T_{Sp}(E)$. Such size changes are coupled to lifetime changes of fluctuations, which can be expressed by the counterpart of Equation (15b):

$$\tau_{fl.}(T) = \tau_0 \left| T - T_{Sp}(E) \right|^{-\phi}. \quad (44)$$

Also, in the given case, the terminal values are related to the condition $\xi(T) \sim l_{grain}$. For the mean-field characterization of the system, the collective and single-element relaxation times are related, i.e., $\tau_{fl.} \propto \tau$. Therefore, the size distribution of grain and the topology, as well as the influence of random local electric fields, must lead to a broad distribution of relaxation times, which is the necessary prerequisite for the glassy dynamics observed in relaxor ceramics, including non-Debye and super-Arrhenius (SA) dynamics.

It is also worth noting that the presented model also explains another characteristic of relaxor ceramics: in different systems, the terminal values of the primary relaxation time range from seconds to milliseconds [1–52]. For the reference dynamics in glass-forming systems, $\tau(T_g) \approx 100$ s [54–56].

Experimental studies complemented the model discussion for relaxor ceramics. They were supported by innovative distortions-sensitive and derivative-based data analysis. This was possible due to the specific characteristics of the experiment and the collected data (see Appendix A). Experimental tests were carried out on a $Ba_{0.65}Sr_{0.35}TiO_3$ relaxor ceramic (see Table 1). Figure 5 shows that the permanent increase in the "dielectric constant" takes place from $T \approx 120$ K to the maximum reached at $T_m \approx 291$ K, and subsequently $\varepsilon(T)$ decreases down to $T_m \approx 375$ K. The typical analysis applies a $1/\varepsilon(T)$ vs. T plot to test the Curie–Weiss (Equation (1)) representation. Such a plot is also shown in Figure 5,

suggesting the CW portrayal covers a range from $T_m \sim 292$ K to $T \approx 228$ K, i.e., for ~ 60 K. in the ferroelectric phase. In the paraelectric phase, which is the particular focus of studies recalling the model analysis, the CW-type (Equation (1)) behavior starts at $T_B \sim 235$K (the Burns temperature) and terminates at $T > 375$ K, i.e., for at least $\Delta T \sim 40$ K. The $\Delta T = T_B - T_m$ is often considered as one of the metrics of the relaxor-type behavior, indicating the width of the domain that deviates from the CW behavior and is associated with the appearance of polar nanoregions (PNRs), hypothetically responsible for the unique behavior [2–4,24]. For the given case, $\Delta T \approx 40$ K. However, the quality of experimental data enables an effective distortions-sensitive and derivative-based test of the model portrayal, avoiding a parasitic scatter. Figure 6 shows such an analysis focusing on the validation of the mean-field behavior related to the Curie–Weiss Equations (1a) and (13a,b) with the exponent $\gamma = 1$. The analysis based on Equation (27) explicitly confirms such behavior between $T = 285$ K and $T = 234$ K, i.e., for ~ 50 K in the ferroelectric phase. In the paraelectric phase, the validation of the CW model description is negative (!).

For the paraelectric phase, the exponential relation Equation (30) gives a much better description of $\varepsilon(T)$ changes than the CW relation in the temperature range from 375 K to 316 K, i.e., covering ~ 60 K, as shown in Figure 7. The superiority of the exponential relation (Equation (30)) is demonstrated by the distortions-sensitive analysis (Equations (31) and (32)), with results presented in Figure 8. The exponential relation with the additional temperature term appears on further cooling towards the paraelectric–ferroelectric transition. The obtained scaling patterns in the broad surrounding of the paraelectric–ferroelectric transition are summarized in Table 2.

Table 2. Scaling patterns for temperature changes in "dielectric constant" ($\varepsilon'(T)$) changes in the broad surrounding of the paraelectric–ferroelectric transition in the tested $Ba_{0.65}Sr_{0.35}TiO_3$ relaxor ceramic, specified in Table 1. Note: $T_m \approx 292$ K.

Temperature Range	**234 K < *T* < 285 K (ferro-)**	**285 K < *T* < 314 K (para-ferro)**	**315 K < *T* < 375 K (para-)**
Scaling equation	$\varepsilon(T) = A_C/(T - T_C)$	$\varepsilon(T) = A\exp(c + aT + bT^2)$	$\varepsilon(T) = A\exp(b + aT)$

Other notable results include the "negligible" distance between the domains represented by subsequent scaling relations, the smooth passing of T_m when using the (para-ferro) equation and the fact that the crossover from the (para-) to the (para-ferro) domain is associated with the inclusion of a single, temperature-dependent term in the exponential relation.

The question arises as to whether the behavior obtained in the (para-) and the (para-ferro) states might suggest that the "dielectric constant" changes are related to the so-called Griffiths phase [99,100], which is expected for near-critical systems (especially of mean-field type) in the presence of random impacts. In the present case, this is the randomness associated with a random local electric field between grains that can penetrate and affect their interiors. An additional frustration can be caused by changing the properties of intergranular layers.

The dynamics in the paraelectric phase of the tested $Ba_{0.65}Sr_{0.35}TiO_3$ system are somewhat beyond the typical pattern observed in relaxor systems, showing the SA-type behavior commonly represented by the VFT dependence. Such behavior is also observed, but it terminates at ~ 340 K. The VFT relation can describe it, but the distortions-sensitive analysis prefers the activated-critical description (Equation (20)). At lower temperatures, a new process emerges. The process explicitly shows an Arrhenius-type temperature dependence ($E_a = const$), extending from $T \sim 330$ K to at least $T \sim 230$ K. Interestingly, this unique pattern for the dynamics seems to have a minimal effect on the "dielectric constant" behavior. The above results are supplemented by $tan\delta(T, f)$ behavior, focusing on its physical significance and its supporting importance in testing relaxation processes: see Figures 9, 10 and 14, and Appendix A. Finally, the effect of the electric field on the "dielectric constant" was tested, revealing its strong changes for the relatively moderate electric field intensities/voltages. These features are often expressed in terms of tunability

(Equation (2)) for practical implementations. The knowledge of the relations describing the broad surroundings of the paraelectric–ferroelectric transitions allowed the derivation of relations for the electric field-related tunability temperature changes (Table 2), without "gaps" between subsequent temperature domains.

In conclusion, we would like to emphasize that the discussion presented in this report has shown the link between relaxor ceramics, Critical Phenomena Physics, and Glass Transition Physics. It shows the importance of uniaxiality for the emergence of mean-field type features. This link suggests that the appearance of a random, strong, intergranular electric field leading to the pseudospinodal behavior [59,86] associated with "weakly discontinuous" phase transitions may be responsible for unique features of relaxor ceramics, particularly regarding the "dielectric constant" ($\varepsilon'(T)$). All of this may re-define the meaning of the Burns temperature and polar nanoregions (PNRs) [2–4], suggesting that they are somewhat "effective" and heuristic concepts introduced to explain relaxor systems mystery [2–53].

The proposed model picture also suggests a significant influence of material engineering characteristics on the dielectric properties of dielectric ceramics. This can be related not only to the grain size, composition, and structure but also to the grain sintering pattern, including the relevant temperature, annealing time, and cooling/heating time rates, which can influence the growth of grains and inter-grain layers, important for the local electric field.

Author Contributions: S.J.R. and A.D.-R. were responsible for the concept of the model, paper writing, and the distortions-sensitive analysis; W.B. was responsible for samples preparation and their non-dielectric characterization; J.Ł. carried out BDS studies and prepared a part of Figures and supported final paper preparation; S.S. carried out measurements of dielectric constant under the strong electric field and supported the paper writing; M.S. and F.G. were consulted for samples preparation and their non-dielectric characterizations. All authors have read and agreed to the published version of the manuscript.

Funding: Sylweser J. Rzoska, Weronika Bulejak, Mikołaj Szafran and Feng Gao were supported by the National Science Center (NCN, Poland), project No 2018/30/Q/ST8/00205. Aleksandra Drozd-Rzoska, Szymon Starzonek, amd Joanna Łoś were supported by the National Science Center (NCN, Poland), OPUS grant, ref. 2022/45/B/ST5/04005.

Institutional Review Board Statement: Not applicable.

Informed Consent Statement: Not applicable.

Data Availability Statement: Data are contained within the article.

Conflicts of Interest: The authors declare no conflict of interest.

Appendix A

The complete set of BDS spectra are presented as the real (ε') and imaginary (ε'') parts of the complex dielectric permittivity in a function of frequency (Figure A1) and the dielectric loss tangent tan δ as a function of frequency. The tests were carried out for about 250 temperatures. For each temperature, 63 frequencies were tested, detecting impedance components with 6-digit resolution.

To supplement the discussion related to $tan\delta$ in the main text of the report, we would like to stress that it is linked to energy, which can be disseminated as heat [55,58,94–96]:

$$\varepsilon^* = \varepsilon' - i\varepsilon'' = \varepsilon'(1 - i \times tan\delta), \tag{A1}$$

$$tan\delta = \frac{\sigma}{\omega\varepsilon} = \frac{loss_current}{charging\ current}, \tag{A2}$$

$$D = tan\delta = \frac{i_{loss}}{i_{loss} + I} = \frac{1}{\omega RC} = \frac{\omega^{\varepsilon''} + \sigma}{\omega\varepsilon'} = \frac{1}{Q}, \tag{A3}$$

leading to the power loss:

$$P = Qtan\delta = \omega CV^2 tan\delta = \varepsilon_0 \varepsilon'' E^2. \quad \text{(A4)}$$

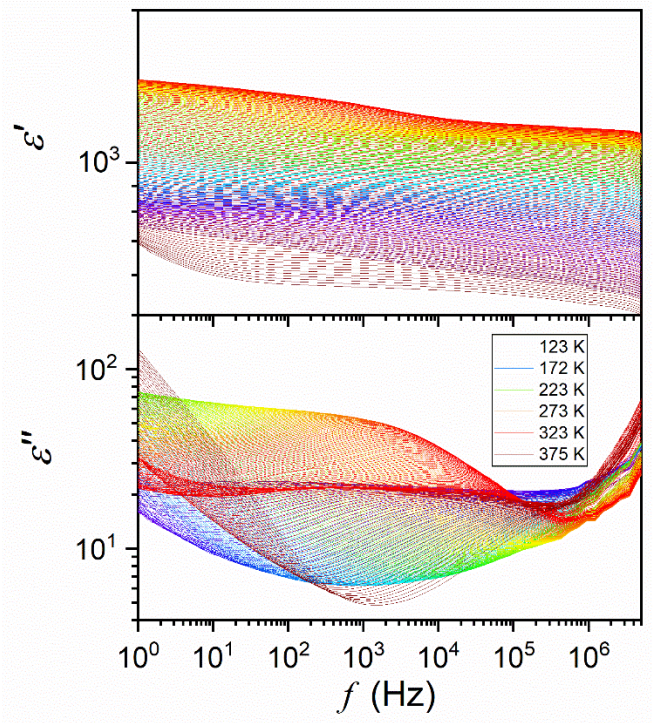

Figure A1. The presentation of detected complex dielectric permittivity spectra for the tests relaxor ceramic $Ba_{0.65}Sr_{0.35}TiO_3$ in the tested temperature range, indicated in the figure.

The latter relation is supplemented by the discussion presented in Refs. [56,96], and shows that the maximum of the loss curve (ε''_{max}, ε''_{peak}, ε''_{m}) directly expresses the maximal energy loss associated with the given relaxation process.

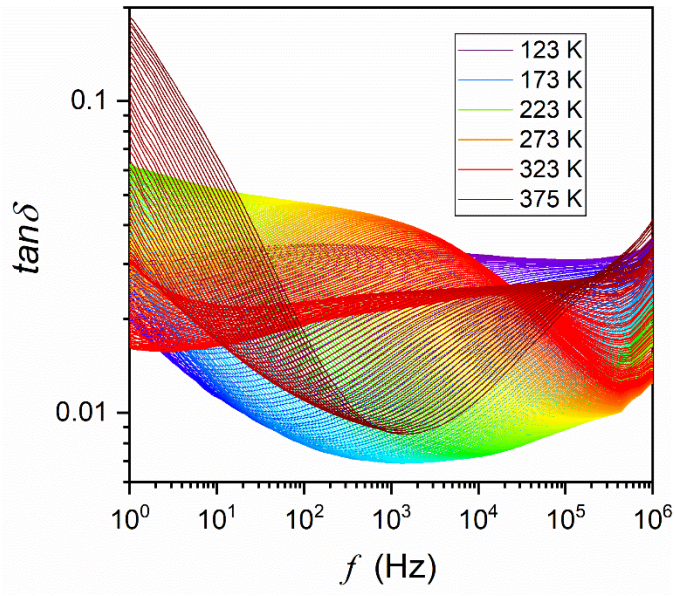

Figure A2. The presentation of detected BDS spectra shown via *tanδ* frequency scans, in the tested temperature range (indicated in the figure) for the relaxor ceramic $Ba_{0.65}Sr_{0.35}TiO_3$, specified in Table 1.

References and Note

1. Smolenskii, G.A.; Rozgachev, K.I. Segnetoelektricheskie svoistva tverdykh rastvorov v sisteme titanat bariya titanat strontsiya (in English: Ferroelectric properties of solid solutions in barium strontium titanate system). *Z. Tekhn. Fiz.* **1954**, *24*, 1751–1760.
2. Uchino, K.; Nomura, S. Critical exponents of the dielectric constants in diffused-phase-transition- crystals. *Ferroelectrics* **1982**, *44*, 55–61. [CrossRef]
3. Burns, G.; Dacol, F.H. Crystalline ferroelectrics with glassy polarization behavior. *Phys. Rev. B* **1983**, *28*, 2527–2529. [CrossRef]
4. Burns, G.; Dacol, F.H. Ferroelectrics with a glassy polarization phase. *Ferroelectrics* **1990**, *104*, 25–35. [CrossRef]
5. Westphal, V.; Kleemann, W.; Glinchuk, M.D. Diffuse phase-transitions and random-field-induced domain states of the relaxor ferroelectric $PbMg_{1/3}Nb_{2/3}O_3$. *Phys. Rev. Lett.* **1992**, *68*, 847–850. [CrossRef]
6. Tagantsev, A.K. Vogel-Fulcher relationship for the dielectric permittivity of relaxor ferroelectrics. *Phys. Rev. Lett.* **1994**, *72*, 1100–1103. [CrossRef]
7. Cheng, Z.-Y.; Katiyar, R.S.; Yao, X.; Bhalla, A.S. Temperature dependence of the dielectric constant of relaxor ferroelectrics. *Phys. Rev. B* **1998**, *57*, 8166. [CrossRef]
8. Pirc, R.; Blinc, R. Spherical random-bond-random-field model of relaxor ferroelectrics. *Phys. Rev. B* **1999**, *60*, 13470–13478. [CrossRef]
9. Tang, X.G.; Chew, K.-H.; Chan, H.L.W. Diffuse phase transition and dielectric tunability of $Ba(Zr_yTi_{1-y})O_3$ relaxor ferroelectric ceramics. *Acta Mater.* **2004**, *52*, 5177–5183. [CrossRef]
10. Poplavko, Y.M. The nature of high dielectric constant in relaxor ferroelectric. *Ferroelectrics* **2004**, *298*, 253–259. [CrossRef]
11. Du, H.; Zhou, W.; Luo, F.; Zhu, D.; Qu, S.; Pei, Z. Phase structure, dielectric properties, and relaxor behavior of $(K_{0.5}Na_{0.5})NbO_3$–$(Ba_{0.5}\ Sr_{0.5})TiO_3$ lead-free solid solution for high temperature applications. *J. Appl. Phys.* **2009**, *105*, 124104. [CrossRef]
12. Cowley, R.A.; Gvasaliya, S.N.; Lushnikov, S.G.; Roessli, B.; Rotaru, G.M. Relaxing with relaxors: A review of relaxor ferroelectrics. *Adv. Phys.* **2011**, *60*, 229–327. [CrossRef]
13. Bokov, A.A.; Ye, Z.-G. Dielectric relaxation in relaxor ferroelectrics. *J. Adv. Dielectr.* **2012**, *2*, 1241010. [CrossRef]
14. Peláiz-Barranco, A.; Calderón-Piñar, F. *Relaxor Behaviour in Ferroelectric Ceramics, Advances in Ferroelectrics*; IntechOpen: Rijeka, Croatia, 2012; pp. 85–107. [CrossRef]
15. Zhang, Q.; Zhai, J.; Kong, L.B. Relaxor ferroelectric materials for microwave tunable applications. *J. Adv. Diel.* **2012**, *2*, 1230002. [CrossRef]
16. Blinc, R. Relaxor ferroelectrics. In *Advanced Ferroelectricity*; International Series of Monographs on Physics; Oxford Academic: Oxford, UK, 2011; pp. 144–186. [CrossRef]
17. Sherrington, D. BZT: A soft pseudospin glass. *Phys. Rev. Lett.* **2013**, *111*, 227601. [CrossRef] [PubMed]
18. Phelan, D.; Stock, C.; Rodriguez-Rivera, J.A.; Chi, S.; Leão, J.; Long, X.; Xie, Y.; Bokov, A.; Ye, Z.-G.; Ganesh, P.; et al. Role of random electric fields in relaxors. *Proc. Natl. Acad. Sci. USA* **2014**, *111*, 1754–1759. [CrossRef]
19. Mydosh, J.A. Spin glasses: Redux: An updated experimental/materials survey. *Rep. Prog. Phys.* **2015**, *78*, 52501. [CrossRef]
20. Guo, H.; Liu, X.; Xue, F.; Chen, L.Q.; Hong, W.; Tan, X. Disrupting long-range polar order with an electric field. *Phys. Rev. B* **2016**, *93*, 174114. [CrossRef]
21. Garten, L.; Burch, M.M.; Gupta, A.S.; Haislmaier, R.; Gopalan, V.; Dickey, E.C.; Trolier-McKinstry, S. Relaxor Ferroelectric behavior in barium strontium titanate. *J. Am. Ceram. Soc.* **2016**, *99*, 1645–1650. [CrossRef]
22. Arce-Gamboa, J.R.; Guzmán-Verrí, G.G. Random electric field instabilities of relaxor ferroelectrics. *NPJ Quantum Mater.* **2017**, *2*, 28. [CrossRef]
23. Martín, J.; Iturrospe, A.; Cavallaro, A.; Arbe, A.; Stingelin, N.; Ezquerra, T.A.C.; Mijangos, A. Nogales Relaxations and relaxor-ferroelectric-like response of nanotubularly confined poly(vinylidene fluoride). *Chem. Mater.* **2017**, *29*, 3515–3525. [CrossRef]
24. Uchino, K. (Ed.) Relaxor based ferroelectrics. In *Advanced Piezoelectric Materials: Science and Technology*; Elsevier: Amsterdam, The Netherlands, 2017; pp. 127–153. [CrossRef]
25. Hagiwara, M.; Ehara, Y.; Novak, N.; Khansur, N.H.; Ayrikyan, A.; Webber, K.G.; Fujihara, S. Relaxor-ferroelectric crossover in $(Bi_{1/2}K_{1/2})TiO_3$: Origin of the spontaneous phase transition and the effect of an applied external field. *Phys. Rev. B* **2017**, *96*, 014103. [CrossRef]
26. Krogstad, M.J.; Gehring, P.M.; Rosenkranz, S.; Osborn, R.; Ye, F.; Liu, Y.; Ruff, J.P.C.; Chen, W.; Wozniak, J.M.; Luo, H.; et al. The relation of local order to material properties in relaxor ferroelectrics. *Nat. Mater.* **2018**, *17*, 718–724. [CrossRef] [PubMed]
27. Palneedi, H.; Peddigari, M.; Hwang, G.T.; Jeong, D.Y.; Ryu, J. High-performance dielectric ceramic films for energy storage capacitors: Progress and outlook. *Adv. Funct. Mater.* **2018**, *28*, 1803665. [CrossRef]
28. Bobic, J.D.; Vijatovic Petrovic, M.M.; Stojanovic, B.D. Review of the most common relaxor ferroelectrics and their applications. In *Magnetic, Ferroelectric, and Multiferroic Metal Oxides*; Elsevier: Amsterdam, The Netherlands, 2018; pp. 233–249. [CrossRef]
29. Raddauoi, Z.; El-Kossi, S.; Dhari, J.; Abdelmoula, N.; Taibi, K. Study of diffuse phase transition and relaxor ferroelectric behavior of $Ba_{0.97}Bi_{0.02}Ti_{0.9}Zr_{0.05}Nb_{0.04}O_3$ ceramic. *RSC Adv.* **2019**, *18*, 2412–2425. [CrossRef] [PubMed]
30. Adamchuk, D.; Grigalaitis, R.; Svirskas, S.; Macutkevic, J.; Palaimiene, E.; Banys, J.; Mitoseriu, L.; Canu, G.; Buscaglia, M.T.; Buscaglia, V. Distributions of relaxation times in relaxor ferroelectric $Ba(Ti_{0.8}\ Ce_{0.2})O_3$. *Ferroelectrics* **2019**, *553*, 103–110. [CrossRef]
31. Zhang, L.L.; Huang, Y.N. Theory of relaxor-ferroelectricity. *Sci. Rep.* **2020**, *10*, 5060. [CrossRef] [PubMed]
32. Gao, F.; Zhang, K.; Guo, Y.; Xu, J.; Szafran, M. (Ba, Sr)TiO_3/polymer dielectric composites–progress and perspective. *Prog. Mater. Sci.* **2021**, *121*, 100813. [CrossRef]

33. Henaish, A.M.; Mostafa, M.; Weinstein, I.; Hemeda, O.; Salem, B. Ferroelectric and dielectric properties of strontium titanate doped with barium. *Magnetism* **2021**, *1*, 22–36. [CrossRef]
34. Wang, G.; Lu, Z.L.; Li, Y.; Li, L.H.; Ji, H.F.; Feteira, A.; Zhou, D.; Wang, D.W.; Zhang, S.J.; Reaney, I.M. Electroceramics for high-energy density capacitors: Current status and future perspectives. *Chem. Rev.* **2021**, *121*, 6124–6172. [CrossRef]
35. Kumar Pradhan, L.; Kar, M. *Relaxor Ferroelectric Oxides: Concept to Applications*; IntechOpen: Rijeka, Croatia, 2021; p. 212021. [CrossRef]
36. Xie, A.; Fu, J.; Zuo, R.; Jiang, X.; Li, T.; Fu, Z.; Yin, Y.; Li, X.; Zhang, S. Supercritical relaxor nanograined ferroelectrics for ultrahigh-energy-storage capacitors. *Adv. Mater.* **2022**, *34*, 2204356. [CrossRef]
37. Shi, X.; Wang, J.; Xu, J.; Cheng, X.; Huang, H. Quantitative investigation of polar nanoregion size effects in relaxor ferroelectrics. *Acta Mater.* **2022**, *237*, 118147. [CrossRef]
38. Vendrell, X.; Ramírez-González, J.; Ye, Z.-G.; West, A.R. Revealing the role of the constant phase element in relaxor ferroelectrics. *Commun. Phys.* **2022**, *5*, 9. [CrossRef]
39. Macutkevič, J.; Banys, J.; Kania, A. Electrical Conductivity and Dielectric Relaxation in $Ag_{1-x}LixNbO_3$. *Crystals* **2022**, *12*, 158. [CrossRef]
40. Jayakrishnan, A.R.; Silva, J.P.B.; Kamakshi, K.; Dastan, D.; Annapureddy, V.; Pereira, M.; Sekhar, K.C. Are lead-free relaxor ferroelectric materials the most promising candidates for energy storage capacitors? *Prog. Mater. Sci.* **2022**, *132*, 101046. [CrossRef]
41. Dwivedi, A.; Singh, K.N.; Hait, M.; Bajpai, P.K. Ferroelectric relaxor behavior and dielectric relaxation in strontium barium niobate—A lead-free relaxor ceramic material. *Eng. Sci.* **2022**, *20*, 117–124. [CrossRef]
42. Hong, Z.; Ke, X.; Wang, D.; Yang, S.; Ren, X.; Wang, Y. Role of point defects in the formation of relaxor ferroelectrics. *Acta Mater.* **2022**, *225*, 117558. [CrossRef]
43. Badole, M.; Dwivedi, S.; Vasavan, H.N.; Saxena, S.; Srihari, V.; Kumar, S. Improved dielectric and relaxor behavior in $LaScO_3$-doped $K_{0.5}Bi_{0.5}TiO_3$ ceramics. *J. Mater. Sci. Mater. Electron.* **2022**, *33*, 25661–25673. [CrossRef]
44. Zhang, L.; Pu, Y.; Chen, M. Complex impedance spectroscopy for capacitive energy-storage ceramics: A review and prospects. *Mater. Today Chem.* **2023**, *28*, 101353. [CrossRef]
45. Yang, B.; Zhang, Q.; Huang, H.; Pan, H.; Zhu, W.; Meng, F.; Lan, S.; Liu, Y.; Wei, B.; Liu, Y.; et al. Engineering relaxors by entropy for high energy storage performance. *Nat. Energy* **2023**, *8*, 956–964. [CrossRef]
46. Li, Y.; Lin, W.; Yang, B.; Zhang, S.; Zhao, S. Domain dynamics engineering in ergodic relaxor ferroelectrics for dielectric energy storage. *Acta Mater.* **2023**, *255*, 119071. [CrossRef]
47. Filipič, C.; Canu, G.; Pirc, R.; Kutnjak, Z. Glassy properties of the lead-free isovalent relaxor $BaZr_{0.4}Ti_{0.6}O_3$. *Crystals* **2023**, *13*, 1303. [CrossRef]
48. Li, Y.; Rao, R.; Wang, Y.; Du, H.; Shi, J.; Liu, X. Effect of chemical inhomogeneity on the dielectric and impedance behaviors of bismuth sodium titanate based relaxors. *ECS J. Solid State Sci. Technol.* **2023**, *12*, 013005. [CrossRef]
49. Su, X.; Li, J.; Hou, Y.; Yin, R.; Li, J.; Qin, S.; Su, Y.; Qiao, L.; Liu, C.; Bai, Y. Large electrocaloric effect over a wide temperature span in lead-free bismuth sodium titanate-based relaxor ferroelectrics. *J. Mater.* **2023**, *9*, 289–298. [CrossRef]
50. Luo, G.; Zhang, G.; Zhang, Y.; Li, A.; Sun, Y.; Tu, R.; Shen, Q. Wide temperature range of stable dielectric properties in relaxor $BaTiO_3$-based ceramics by co-doping synergistic engineering. *Mat. Chem. Phys.* **2023**, *302*, 127629. [CrossRef]
51. Chen, X.; Qin, H.; Zhu, W.; Zhang, B.; Lu, W.; Bernholc, J.; Zhang, Q.M. Giant electrostriction enabled by defect-induced critical phenomena in relaxor ferroelectric polymers. *Macromolecules* **2023**, *56*, 690–696. [CrossRef]
52. Sojecka, A.A. The Search and Analysis Carried out for This Report, Using Google Scholar Database. (accessed on 15 October 2023).
53. Market Research Report: Relaxor Ferroelectric Ceramics Sales Market Research Report (DataIntelo, 2022.id 2863). Available online: https://dataintelo.com/report/global-relaxor-ferroelectric-ceramics-sales-market/ (accessed on 15 October 2023).
54. Donth, E. *Glass Transition: Relaxation Dynamics in Liquids and Disordered Solids*; Springer: Berlin/Heidelberg, Germany, 2001; ISBN 978-3540418016.
55. Kremer, F.; Schoenhals, A. *Broadband Dielectric Spectroscopy*; Springer: Berlin/Heidelberg, Germany, 2003; ISBN 978-3642628092.
56. Drozd-Rzoska, A.; Rzoska, S.J.; Starzonek, S. New scaling paradigm for dynamics in glass-forming systems. *Prog. Mat. Sci.* **2023**, *134*, 101074. [CrossRef]
57. Jonsher, A.K. *Dielectric Relaxation in Solids*; Chelsea Dielectric Press: London, UK, 1983; ISBN 9780950871103.
58. Łoś, J.; Drozd-Rzoska, A.; Rzoska, S.J. Critical-like behavior of low-frequency dielectric properties in compressed liquid crystalline octyloxycyanobiphenyl (8OCB) and its nanocolloid with paraelectric $BaTiO_3$. *J. Mol. Liq.* **2023**, *377*, 121555. [CrossRef]
59. Stanley, H.E. *Introduction to Phase Transition and Critical Phenomena*; Oxford University Press: New York, NY, USA, 1992; ISBN 978-0195053166.
60. Domb, C.; Lebovitz, J. *Phase Transitions and Critical Phenomena*; Academic Press: New York, NY, USA, 1984; Volume 9, ISBN 0122203097.
61. Anisimov, M.A. *Critical in Liquids and Liquid Crystals*; Gordon and Breach: Reading, UK, 1992.
62. Drozd-Rzoska, A.; Rzoska, S.J.; Kalabiński, J. The impact of pressure on low molecular weight near-critical mixtures of limited miscibility. *ACS Omega* **2020**, *5*, 20141–20152. [CrossRef]
63. Murray, C. *Ferroelectric Materials: Science and Technology*; States Academic Press: Cambridge, UK, 2022; ISBN 978-1639891986.
64. Rabe, K.M.; Ahn, C.H. *Physics of Ferroelectrics: A Modern Perspective*; Springer: Berlin/Heidelberg, Germany, 2007; ISBN 978-3540345909.
65. Editorial: A century of ferroelectricity. *Nat. Mater.* **2020**, *19*, 129. [CrossRef]
66. Editorial. Ferroelectricity: 100 Years on. Physics World. Issue 10 November 2021. Available online: https://physicsworld.com/a/ferroelectricity-100-years-on/ (accessed on 15 October 2023).

67. Blinc, R.; Musevic, I.; Zeks, B. *The Physics of Ferroelectric and Antiferroelectric Liquid*; World Scientific: Singapore, 2000.
68. Guo, Q.; Yan, K.; Chigrinov, V.; Zhao, H.; Tribelsky, M. Ferroelectric Liquid Crystals: Physics and Applications. *Crystals* **2019**, *9*, 470. [CrossRef]
69. Mugiraneza, S.; Hallas, A.M. Tutorial: A beginner's guide to interpreting magnetic susceptibility data with the Curie-Weiss law. *Commun. Phys.* **2022**, *5*, 95. [CrossRef]
70. Jonker, G.H. On dielectric Curie-Weiss law and diffuse phase transition in ferroelectrics. *Mat. Res. Bull.* **1983**, *18*, 301–308. [CrossRef]
71. Trainer, M. Ferroelectrics and the Curie–Weiss law. *Eur. J. Phys.* **2000**, *21*, 459–464. [CrossRef]
72. Devonshire, A.F. Theory of ferroelectrics. *Adv. Phys.* **1954**, *3*, 85–130. [CrossRef]
73. Levanlyuk, A.; Misirlioglu, I.B.; Okatan, M.B. Landau, Ginzburg, Devonshire and others. *Ferroelectrics* **2020**, *569*, 310–323. [CrossRef]
74. Landau, L.D.; Lifshitz, E.M. *Statisticheskaya Fizika (Statistical Physics)*; GTTI: Moscow, Russia, 1938.
75. Honig, J.M.; Spalek, J. *A Primer to the Theory of Critical Phenomena*; Elsevier: Amsterdam, The Netherlands, 2020; ISBN 978-0128046852.
76. Kumar, A.; Krishnamurthy, H.R.; Gopal, E.S.R. Equilibrium critical phenomena in binary liquid mixtures. *Phys. Rep.* **1983**, *98*, 57–143. [CrossRef]
77. Bausch, R. Ginzburg criterion for tricritical points. *Z. Phys.* **1972**, *254*, 81–88. [CrossRef]
78. Als-Nielsen, J.; Birgeneau, R.J. Mean field theory, the Ginzburg criterion, and marginal dimensionality of phase transitions. *Am. J. Phys.* **1977**, *45*, 54–56. [CrossRef]
79. Beysens, D.; Gbadamassi, M.; Boyer, L. Light-scattering study of a critical mixture with shear flow. *Phys. Rev. Lett.* **1979**, *43*, 1253. [CrossRef]
80. Beysens, D.; Gbadamassi, M. Shear-induced transition to mean-field critical behavior. *J. Phys. Lett.* **1979**, *40*, 565–567. [CrossRef]
81. Chan, C.K.; Lin, L. Effects of shear on the phase transition of binary mixtures. *EPL* **1990**, *11*, 13–18. [CrossRef]
82. Baumberger, T.; Perrot, F.; Beysens, D. Shear flow effects on a critical binary mixture during phase separation. *Phys. A* **1991**, *174*, 31–46. [CrossRef]
83. Drozd-Rzoska, A. Shear viscosity studies above and below the critical consolute. point in a nitrobenzene-decane mixture. *Phys. Rev. E* **2000**, *62*, 8071–8074. [CrossRef] [PubMed]
84. Rzoska, S.J. Kerr effect and nonlinear dielectric effect on approaching the critical consolute point. *Phys. Rev. E* **1993**, *48*, 1136–1143. [CrossRef] [PubMed]
85. Drozd-Rzoska, A.; Rzoska, S.J.; Martinez-Garcia, J.C. Nonlinear dielectric effect in supercritical diethyl ether. *J. Chem. Phys.* **2014**, *141*, 094907. [CrossRef] [PubMed]
86. Chrapeć, J.; Rzoska, S.J.; Zioło, J. Pseudospinodal curve for binary solutions determined from the nonlinear dielectric effect. *Chem. Phys.* **1987**, *111*, 155–160. [CrossRef]
87. Drozd-Rzoska, A.; Rzoska, S.J.; Starzonek, S. New paradigm for configurational entropy in glass forming liquids. *Sci. Rep.* **2022**, *12*, 3058. [CrossRef]
88. Starzonek, S.; Zhang, K.; Drozd-Rzoska, A.; Rzoska, S.J.; Pawlikowska, E.; Szafran, M.; Gao, F. Polyvinylidene difluoride-based composite: Glassy dynamics and pretransitional behaviour. *Eur. Phys. J.* **2020**, *93*, 55. [CrossRef]
89. Levit, R.; Martinez-Garcia, J.C.; Ochoa, D.A.; García, J.E. The generalized Vogel-Fulcher-Tamman equation for describing the dynamics of relaxor ferroelectrics. *Sci. Rep.* **2019**, *9*, 12390. [CrossRef]
90. Drozd-Rzoska, A. Universal behavior of the apparent fragility in ultraslow glass forming systems. *Sci. Rep.* **2019**, *9*, 6816. [CrossRef]
91. Drozd-Rzoska, A.; Rzoska, S.J.; Paluch, M. Universal critical-like scaling of dynamic properties in symmetry-selected glass formers. *J. Chem. Phys.* **2008**, *129*, 184509. [CrossRef] [PubMed]
92. Colby, R.H. Dynamic scaling approach to glass formation. *Phys. Rev. E* **2000**, *61*, 1783–1791. [CrossRef]
93. Hirshfeld, A. *The Electric Life of Michael Faraday*; Raincoast Books: New York, NY, USA, 2006; ISBN 978-1551929453.
94. Arelli, S.G. *Dielectric Materials: Types of Dielectrics, Various Polarizations, Clausius Mossotti Relation, Classical Theory of Electronic Polarizability*; Independently Publisher: Traverse City, MI, USA, 2021; ISBN 979-8598251652.
95. Von Hippel, R. *Dielectrics and Waves*; Chapman & Hall: New York, NY, USA, 1954.
96. Chełkowski, A. *Dielectric Physics*; PWN-Elsevier: Warsaw, Poland, 1990; ISBN 978-044499766.
97. Starzonek, S.; Rzoska, S.J.; Drozd-Rzoska, A.; Pawlus, S.; Biała, E.; Cesar Martinez-Garcia, J.; Kistersky, L. Fractional Debye-Stokes-Einstein behaviour in an ultraviscous nanocolloid: Glycerol and silver nanoparticles. *Soft Matter* **2015**, *11*, 5554–5562. [CrossRef]
98. Fugiel, B.; Ćwikiel, K.; Zioło, J. Gap exponents determined from the pressure measurements of the nonlinear electric permittivity for triglycine sulfate in the paraelectric region. *Phys. Rev. B* **1987**, *36*, 3963–3964. [CrossRef] [PubMed]
99. Griffiths, R.B. Nonanalytic behavior above the critical point in a random Ising ferromagnet. *Phys. Rev. Lett.* **1969**, *23*, 17. [CrossRef]
100. Voyta, T. Phases and phase transitions in disordered quantum systems. *AIP Conf. Proc.* **2013**, *1550*, 188–247. [CrossRef]

Disclaimer/Publisher's Note: The statements, opinions and data contained in all publications are solely those of the individual author(s) and contributor(s) and not of MDPI and/or the editor(s). MDPI and/or the editor(s) disclaim responsibility for any injury to people or property resulting from any ideas, methods, instructions or products referred to in the content.